

# Superposition of Cretaceous and Cenozoic deformation in northern Tibet: A far-field response to the tectonic evolution of the Tethyan orogenic system

Ye Wang<sup>1</sup>, Xuanhua Chen<sup>1,†</sup>, Yaoyao Zhang<sup>1,†</sup>, Zheng Yin<sup>2</sup>, Andrew V. Zuza<sup>3</sup>, An Yin<sup>4</sup>, Yongchao Wang<sup>1</sup>,  
Weicui Ding<sup>1</sup>, Shenglin Xu<sup>1</sup>, Yiping Zhang<sup>1</sup>, Bing Li<sup>1</sup>, and Zhaogang Shao<sup>1</sup>

<sup>1</sup>*SinoProbe Center, Chinese Academy of Geological Sciences and China Geological Survey, Beijing 100037, China*

<sup>2</sup>*Administration of Natural Resources of Zhangye City, Zhangye, Gansu 734000, China*

<sup>3</sup>*Nevada Bureau of Mines and Geology, University of Nevada, Reno, Nevada 89557, USA*

<sup>4</sup>*Department of Earth, Planetary, and Space Sciences, University of California, Los Angeles, California 90095, USA*

## ABSTRACT

Although the Cenozoic Indo-Asian collision is largely responsible for the formation of the Tibetan plateau, the role of pre-Cenozoic structures in controlling the timing and development of Cenozoic deformation remains poorly understood. In this study we address this problem by conducting an integrated investigation in the northern foreland of the Tibetan plateau, north of the Qilian Shan-Nan Shan thrust belt, NW China. The work involves field mapping, U-Pb detrital-zircon dating of Cretaceous strata in the northern foreland of the Tibetan plateau, examination of growth-strata relationships, and construction and restoration of balanced cross sections. Our field mapping reveals multiple phases of deformation in the area since the Early Cretaceous, which was expressed by northwest-trending folding and northwest-striking thrusting that occurred in the early stages of the Early Cretaceous. The compressional event was followed immediately by extension and kinematically linked right-slip faulting in the later stage of the Early Cretaceous. The area underwent gentle northwest-trending folding since the late Miocene. We estimate the magnitude of the Early Cretaceous crustal shortening to be ~35%, which we interpret to have resulted from a far-field response to the collision between the Lhasa and the Qiangtang terranes in the south. We suggest that the subsequent extension in the Early Cretaceous was


induced by orogenic collapse. U-Pb dating of detrital zircons, sourced from Lower Cretaceous sedimentary clasts from the north and the south, implies that the current foreland region of the Tibetan plateau was a topographic depression between two highland regions in the Early Cretaceous. Our work also shows that the Miocene strata in the foreland region of the northern Tibetan plateau was dominantly sourced from the north, which implies that the rise of the Qilian Shan did not impact the sediment dispersal in the current foreland region of the Tibetan plateau where this study was conducted.

## INTRODUCTION

One of the important questions with regard to the development of the Tibetan plateau is whether its current high topography was constructed entirely during the Cenozoic Indo-Asian collision (e.g., England and Houseman, 1986; Tapponnier et al., 2001; Wang et al., 2008) or a superposed result of Cenozoic and pre-Cenozoic crustal shortening (e.g., Murphy et al., 1997). The first scenario predicts the Qilian Shan of northernmost Tibet was a lowland in the Cretaceous, with an elevation similar to that of a typical stable craton at an elevation of ~500 m (e.g., England and Houseman, 1986); its current high topography did not appear until the late Cenozoic after ca. 20–15 Ma (e.g., Tapponnier et al., 2001). The second scenario implies that parts of the Tibetan plateau could have been higher than the average elevation of a typical craton because the region experienced multiple tectonic events related to subduction, ocean closure, and terrane collision during the development of the Tethys orogenic system (Murphy et al., 1997; Jolivet et al., 2001; Kapp et al., 2003, 2007; Li et al.,

2019a, 2020a; Zhao et al., 2020). Although the hypothesis of a proto-plateau in southern Tibet has been carefully investigated (Murphy et al., 1997; Kapp et al., 2003), the possibility that the northern Tibetan plateau may have also been a highland region immediately prior to the Cenozoic Indo-Asian collision has never been thoroughly investigated. Yet, the existence of such a proto-highland region in northern Tibet has important implications for the current understanding of the relationship between the Tibetan-plateau formation and climate change in Asia (e.g., Raymo and Ruddiman, 1992; Licht et al., 2014). It also has implications for mass-balance calculations and estimates of total crustal shortening for the Cenozoic construction of the Tibetan plateau (e.g., van Hinsbergen et al., 2011; Yakovlev and Clark, 2014; Zuza et al., 2016).

The northern margin of the Tibetan plateau is marked by the northwest-trending Qilian Shan that hosts the early Paleozoic Qilian orogen (Fig. 1) (e.g., Şengör and Natal'in, 1996a; Yin and Harrison, 2000; Heubeck, 2001; Stampfli and Borel, 2002; Yin et al., 2007; Stampfli et al., 2013; Xiao et al., 2015; Wu et al., 2016, 2020a, 2020b; Zuza and Yin, 2016; Zuza et al., 2018). Because the Qilian Shan is the site of the early Paleozoic orogen (e.g., Şengör and Natal'in, 1996b; Yang et al., 2002; Yin and Harrison, 2000; Xiao et al., 2009; Song et al., 2013; Zuza et al., 2018) and a Cenozoic thrust belt (Yin et al., 2002, 2008a, 2008b; Zuza et al., 2016, 2019), previous geologic research has focused exclusively on the timing and processes of these two most dominant geologic events in the region (e.g., Yin and Harrison, 2000; Gehrels et al., 2003a, 2003b; Yin, 2010). With a few exceptions (e.g., Vincent and Allen, 1999; Jolivet et al., 2001; Chen et al., 2003; Gehrels et al., 2011), the intervening

Xuanhua Chen  <https://orcid.org/0000-0003-3328-1892>

<sup>†</sup>Corresponding authors: xhchen@cags.ac.cn; zhangyy@cags.ac.cn.

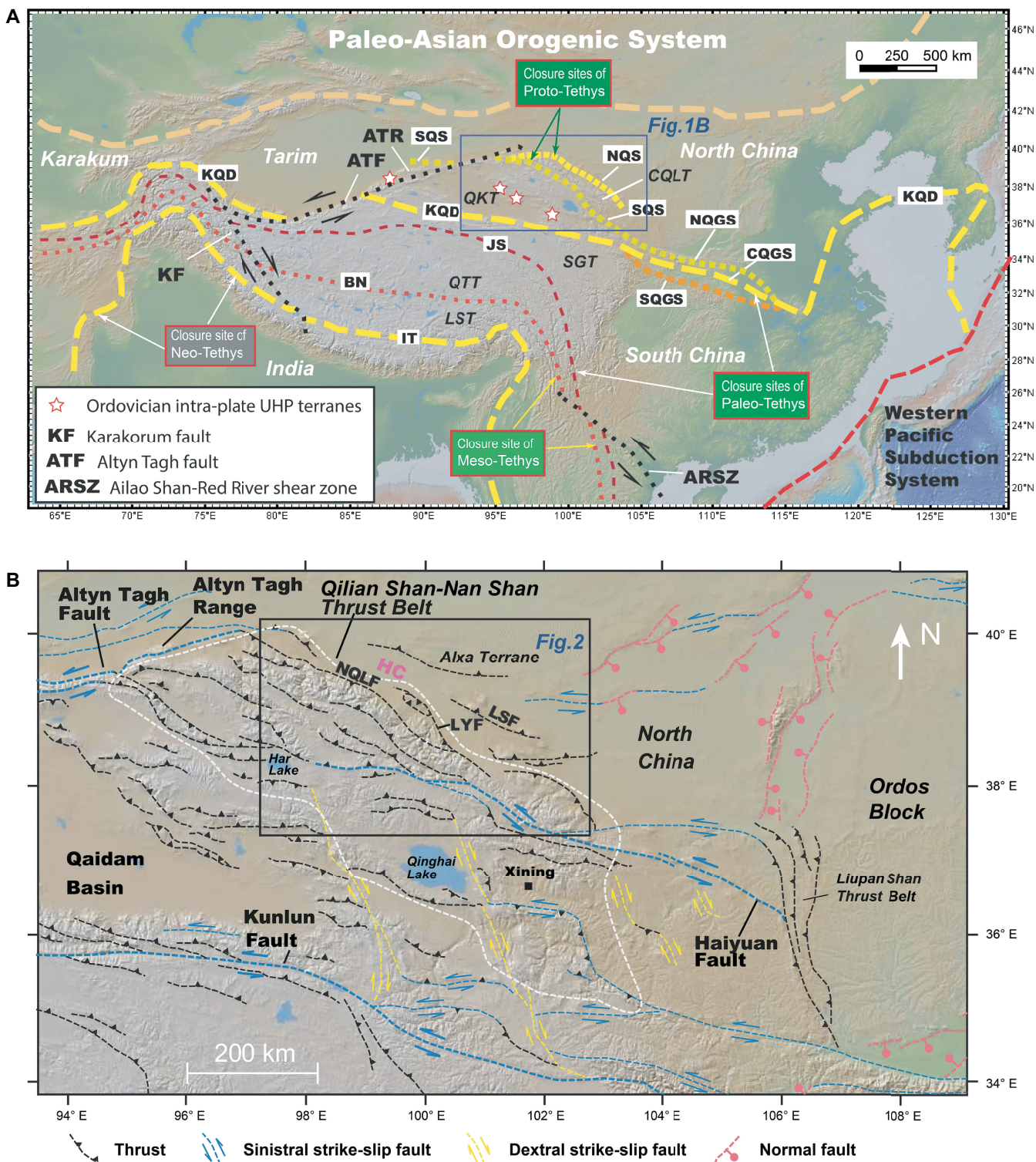


**Figure 1.** (A) Tectonic map of the Tethyan and the Paleo-Asian orogenic systems (modified from Wu et al., 2016, 2017). UHP—ultra high pressure. KQD—Kunlun-Qinling-Dabie suture; NQS and SQS—North and South Qilian sutures; NQGS, CQGS, and SQGS—North, Central, and South Qinling sutures; JS—Jinsha suture; BN—Bangong-Nujiang suture; IT—Indus-Tsangpo suture. QKT—Qaidam-Kunlun terrane; SGT—Songpan-Ganzi terrane; QTT—Qiangtang terrane; LST—Lhasa terrane; CQLT—Central Qilian terrane. KF—Karakorum fault; ARSZ—Ailao Shan-Red River shear zone; ATF—Altyn Tagh fault. ATR—Altyn Tagh Range. (B) Sketched fault tectonic map of the Qilian Shan-Nan Shan Range and its adjacent regions (modified from Gao et al., 2013; Zuza et al., 2016; Wu et al., 2017). HC—Hexi Corridor; NQLF—North Qilian fault; LYF—Liyuanpu fault; LSF—Longshou Shan fault. Underlying base map is from [www.geomapapp.org](http://www.geomapapp.org) (Ryan et al., 2009).



history between the early Paleozoic Qilian orogeny and Cenozoic construction of the northern Tibetan plateau remains poorly understood. For example, it is unclear if the region was deformed repeatedly in response to the tectonic development of the Tethyan and Paleo-Asian orogenic systems north and south of the Qilian Shan since the end of the Qilian orogeny and the onset of the Indo-Asian collision (Yin and Nie, 1996; Şengör and Natal'in, 1996b; Yin and Harrison, 2000). In this work, we address this issue by examining the structural and stratigraphic relationships of a Cretaceous sequence overlain by Miocene strata. Our detailed field observations allow us to decompose the total deformation magnitude of the Cretaceous strata into Cretaceous and Cenozoic components. We show below that the Lower Cretaceous strata experienced a compressional event and an extensional event in the Cretaceous, followed by a Miocene compressional event. Our provenance analysis assisted by U-Pb dating of detrital zircon suggests that the Lower Cretaceous sediments were sourced from the north and the south, which implies that the current foreland region of the northern Tibetan plateau was a topographic depression between two highland regions in the Early Cretaceous. Our work also shows that the Miocene strata in the foreland region of the Tibetan plateau was dominantly sourced from the north, which implies that the rise of the Qilian Shan did not impact the sediment dispersal in the current foreland region of the Tibetan plateau where this study was conducted.

## REGIONAL GEOLOGY

The Qilian Shan marks the northern margin of the Tibetan plateau and hosts the early Paleozoic Qilian orogen composed of basement and supracrustal rocks of the North China craton and early Paleozoic oceanic-arc and mélange complexes (Pan and Xiao, 2015; Chen et al., 2019a). Some authors considered the Qilian orogen to have been generated by accretionary processes (Yin and Nie, 1996; Yin and Harrison, 2000; Song et al., 2006, 2007, 2013, 2014; Xiao et al., 2009; Yang et al., 2010; Chen et al., 2010, 2019a; Pan and Xiao, 2015), whereas others show that the apparent multi-terrane architecture of the orogen, the basis for the accretionary-orogen hypothesis, is a result of Cenozoic thrust duplication of a single arc-over-continent subduction zone (Yin et al., 2007). The Qilian Shan region experienced Middle to Late Triassic compression (Chen et al., 2019a, 2019b), possibly in response to the closure of the Paleo-Tethyan ocean along the southern margin of the East Kunlun Shan (Chen et al., 2012, 2015; Wu et al., 2016). Two discrete phases of extension have also been documented in the area, one in the Early Jurassic and another in the

Early Cretaceous (Chen et al., 2003; Li, 2003; Chen et al., 2014a; Cheng et al., 2019b). These extensional events were expressed by the formation of extensional and transtensional basins and rapid cooling of fault-bounded footwall rocks (Vincent and Allen, 1999; Chen et al., 2003; Yin et al., 2008a, 2008b; Zuza et al., 2016).

The early Paleozoic orogen was reactivated in the Cenozoic by the development of the Qilian Shan-Nan Shan thrust belt between the North China craton in the north and the Qaidam basin in the south (Figs. 1–3) (Yin and Harrison, 2000; Chen et al., 2003; Wu et al., 2016; Zuza and Yin, 2016; Zuza et al., 2016, 2018, 2019; Zhang et al., 2017a; Li et al., 2019a, 2021; Lin et al., 2019; Yu et al., 2019). Restoration of balanced cross sections across the Qaidam basin and the Qilian Shan-Nan Shan thrust belt indicates >250–350 km of Cenozoic N-S shortening has been occurred in the region (Yin et al., 2008a, 2008b; Zuza et al., 2016). The Qilian Shan-Nan Shan thrust belt are kinematically linked with east-trending left-slip faults and northwest-trending right-slip faults interpreted as a result of a clockwise rotation (Zuza and Yin, 2016). Cenozoic shortening strain is higher (>50%) along the northern margin of the Qilian Shan-Nan Shan thrust belt and lower (>30%–35%) in the thrust belt interior (Zuza et al., 2016). Below, we describe the stratigraphy and structural geology in a foreland region north of the Qilian Shan based on our own field studies and the incorporation of existing work.

## STRATIGRAPHY

Our study area (Figs. 3, 4, and 5) exposes rocks with ages ranging from the Ordovician to the Miocene (Figs. 5 and 6; BGGP, 1971, 1973; BGQP, 1968). Ordovician rocks are composed of meta-sandstone, slates, phyllite, schists, mafic volcanic rocks, chert, limestone, and marble; Silurian strata are mainly meta-greywacke; Devonian strata are dominantly volcanic, pyroclastic, and siliciclastic rocks; and Carboniferous–Permian units are bioclastic and siliceous limestone and fluvial sediments. Triassic and Jurassic strata in the study area are composed of conglomerates, sandstones, siltstones, shale, and coal seams (Fig. 3).

The Lower Cretaceous Xinminpu Formation ( $K_1xm$ ) consists of sandstone, siltstone, and mudstone above a basal layer of pebbly sandstone and conglomerate (Fig. 6; BGGP, 1971, 1973). We divide the Xinminpu Formation ( $K_1xm$ ) into the lower ( $K_1xm^a$ ) and upper ( $K_1xm^b$ ) members (Fig. 6). The lower member ( $K_1xm^a$ ) consists of six sub-units (Fig. 6). Sub-unit 1 ( $K_1xm^{a1}$ ) is a sequence of purple-red and yellow-green conglomerate, glutenite, sandstone, and siltstone interlayered with argillaceous siltstones. Sub-

unit 2 ( $K_1xm^{a2}$ ) comprises pink and gray-green conglomerate, sandstone, argillaceous siltstone, and mudstone. Sub-unit 3 ( $K_1xm^{a3}$ ) is composed of grayish-white, gray-green, yellow-green, and ash-brown pebbly sandstone, sandstone, argillaceous siltstone, and mudstone. Sub-unit 4 ( $K_1xm^{a4}$ ) is a section of brick-red, yellow-green, gray-green, gray-brown, yellow, and orange mudstones. Sub-unit 5 ( $K_1xm^{a5}$ ) consists of light-yellow, yellow-green, and purple-red glutenite, mudstone, pebbly sandstone, and siltstone. Sub-unit 6 ( $K_1xm^{a6}$ ) consists of purple-red and earth-yellow conglomerate, sandstone, and mudstone. The upper member of the Xinminpu Formation ( $K_1xm^b$ ) consists of two sub-units (Fig. 6). The lower sub-unit ( $K_1xm^{b1}$ ) consists of gray-green, taupe, and purple-red pebbly sandstone, glutenite, sandstone, and siltstone. The upper sub-unit ( $K_1xm^{b2}$ ) comprises brick-red, gray-green, and yellow-green sandstone, siltstone, silty mudstone, and mudstone.

The Miocene sequence ( $N_1$ ), which is unconformably on top of the Cretaceous and pre-Cretaceous strata (Figs. 3, 6, and 7), is composed of reddish pebbly sandstone, sandstone, sandy mudstone, and argillaceous siltstone (BGGP, 1971, 1973). The Pliocene unit ( $N_2$ ) is a sequence of interbedded siltstones and conglomerates (Liu et al., 2011). Quaternary units in the study area can be divided into alluvial, diluvial, aeolian, lacustrine, swamp, and chemical deposits (Fig. 3).

## STRUCTURAL GEOLOGY

### Folds

Major folds involving Cretaceous strata are the Daoshan anticline, the Aoheshan syncline, and the Hongshan anticlinorium. The Daoshan anticline is an open and asymmetric fold with its northeast limb dipping more steeply than its southwest limb. It trends S30°E and plunges 24°. The core of the fold consists of conglomerate, glutenite, sandstone, and siltstone of the lower member of the Cretaceous Xinminpu Formation ( $K_1xm^{a1}$ ) (BGGP, 1971, 1973). The northeastern limb has been eroded away, and the remaining part of the fold indicates a wavelength of ~7 km.

The Aoheshan syncline (Figs. 4, 5, and 8) is an open and symmetric fold with limbs dipping at 35°–45°. The fold hinge line trends S58°E and plunges 14°. The fold axial trace can be traced for >9 km. The core of the syncline consists of unit  $K_1xm^{a5}$  and the limbs of the syncline consists of unit  $K_1xm^{a6}$  (the youngest stratigraphic unit involved) in its southeast edge. The wavelength of the fold is ~7 km.

The Hongshan anticlinorium consists of several superimposed folds including a major

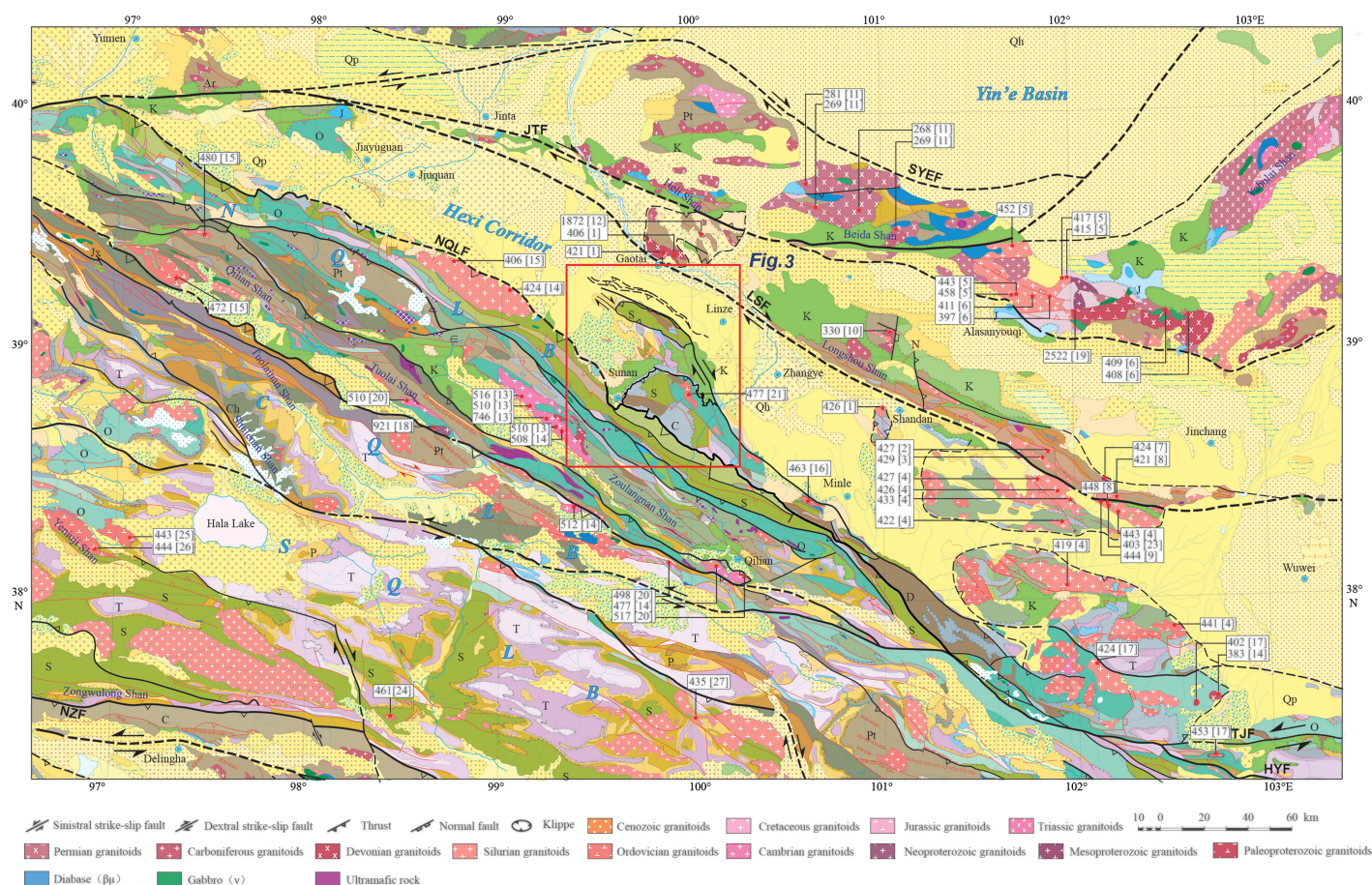


**Figure 2.** Simplified geologic map of the northern Qilian Shan and surrounding regions in NW China—showing simplified fault system and distribution of zircon U-Pb granitoid ages. Modified from China Geological Survey (2004). NQLB—North Qilian Orogenic Belt; CQLB—Central Qilian Orogenic Belt; SQLB—South Qilian Orogenic Belt (Early Paleozoic). Strata systems: Qh—Holocene; Qp—Pleistocene; N—Neogene; E—Paleogene; K—Cretaceous; J—Jurassic; T—Triassic; P—Permian; C—Carboniferous; D—Devonian; S—Silurian; O—Ordovician; E—Cambrian; Pt—Proterozoic. Faults: JTF—Jinta fault; SYEF—South Yin’e fault; NQLF—North Qilian fault; LSF—Longshou Shan fault; NZF—North Zongwulong Shan fault; HYF—Haiyuan fault; TJF—Tianjing Shan fault. U-Pb age data are from: [1] Wang et al. (2020); [2] Zhang et al. (2021); [3] Tang (2015); [4] Zhang et al. (2017b); [5] Liu et al. (2016); [6] Zhou et al. (2016); [7] Duan et al. (2015); [8] Qin (2012); [9] Wei et al. (2013); [10] Xue et al. (2017); [11] Liu et al. (2017b); [12] Wang et al. (2019); [13] Chen et al. (2014b); [14] Wu et al. (2010); [15] Gehrels et al. (2003b); [16] Wu et al. (2006); [17] Xiong et al. (2012); [18] Zuza et al. (2018); [19] Gong et al. (2012); [20] Fu et al. (2020); [21] Song et al. (2013); [22] Tseng et al. (2009); [23] Hu et al. (2005); [24] Liao et al. (2014); [25] Zhang et al. (2018); [26] Yu et al. (2018); [27] Shi et al. (2015). Location of Figure 3 is shown with red rectangle.

anticline. The folds trend from east to south-east and south due to curved axial planes. The averaged fold hinge orientation trends S62°E and plunges 12°. The involved strata are mainly the lower member of the Xinminpu Formation. Locally, smaller parasitic folds with an average fold wavelength of ~150 m are present in unit K<sub>1</sub>xm<sup>b</sup> (Fig. 9). The smaller folds trend ~290°, and their limbs dip gently at 15°–30°.

An anticline involving Miocene strata (N<sub>1</sub>) trends S21°W and plunges 12°. It is an asymmetric fold superimposed on older Cretaceous folds (Figs. 5, 10B, and 11). The northwestern fold limb dips ~13°, whereas the southeastern fold limb dips 44°–55°.

## Faults

The study area exposes the Liyuanpu, Lanheba, Gaerwan, Hongshan, Nianpangou, Aohe, and Qijiazaizi faults (Fig. 5). The north-west-striking Liyuanpu fault dips 70°–80° NE. It truncates the Lower Cretaceous Xinminpu Formation (Fig. 5). The fault extends >80 km and merges with the North Qilian thrust at its southeastern end (Figs. 1B and 3). The Liyuanpu fault and folds in Cretaceous strata are covered by Miocene deposits (N<sub>1</sub>) (Figs. 5 and 10). Several branches of the Liyuanpu fault system are mapped in the study area, which include the Gaoerwan, Donghe, and Lanheba faults (Figs. 4 and 5). The Liyuanpu fault system truncates the

Yumushan thrust and nappe system (Chen et al., 2019b) (Fig. 3). The total displacement along the Liyuanpu fault is unknown.

The Lanheba fault is a branching structure of the Liyuanpu fault (Figs. 4, 5, 10A, and 10B), striking ~320° and dipping 75° to N50°E. The fault can be traced for ~5.5 km. Right-separation of a marker bed for ~70 m occurs along the fault (Figs. 10A and 10B). Farther southeast, the magnitude of right-separation along the fault increases from ~150 m to ~900 m, and finally reaching to ~1.3 km. The fault manifests as a thrust fault, resulting in strata thickening in unit K<sub>1</sub>xm<sup>a2</sup>. The west-northwest-striking Gaoerwan fault is also a branching structure of the Liyuanpu fault,



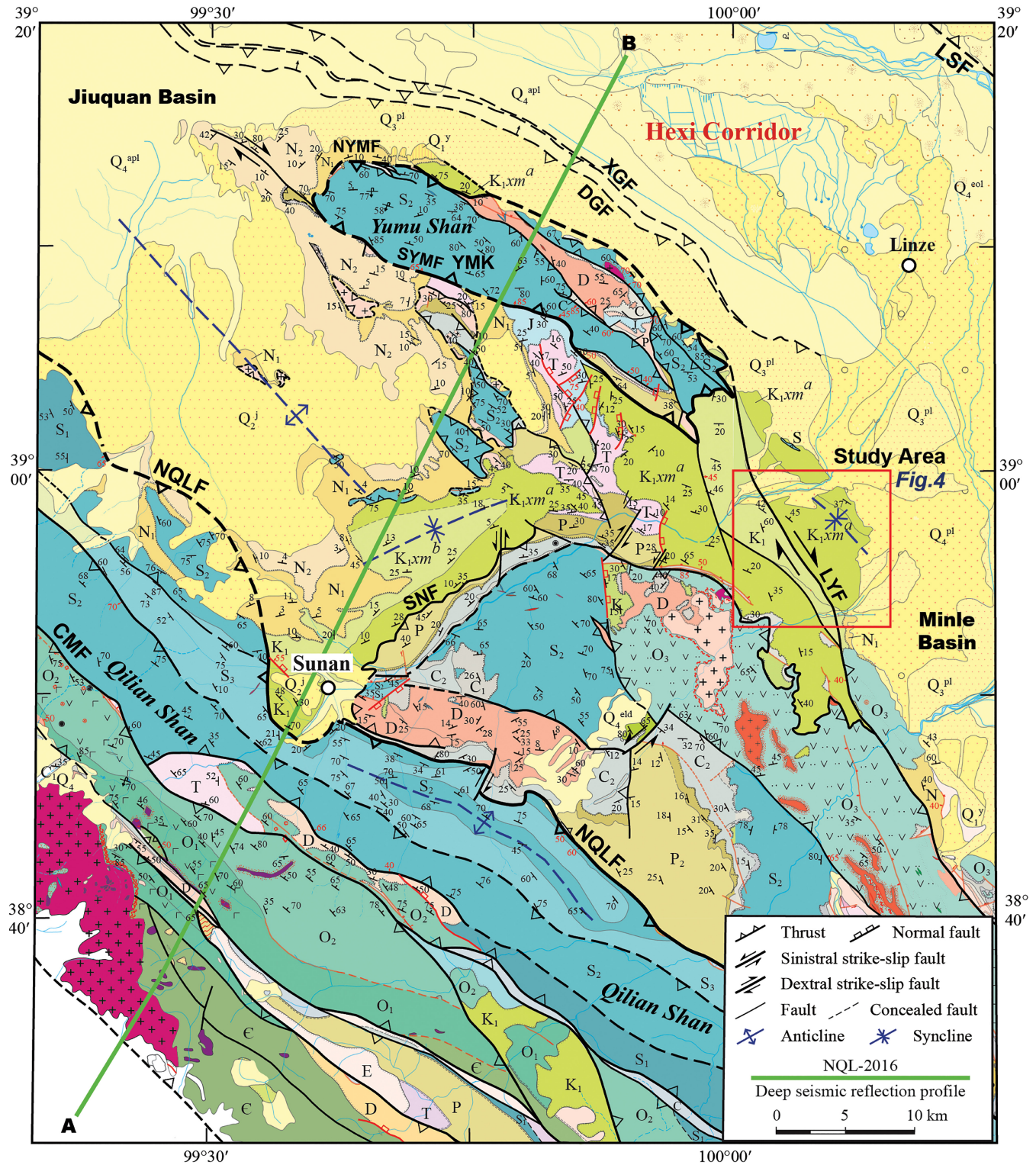
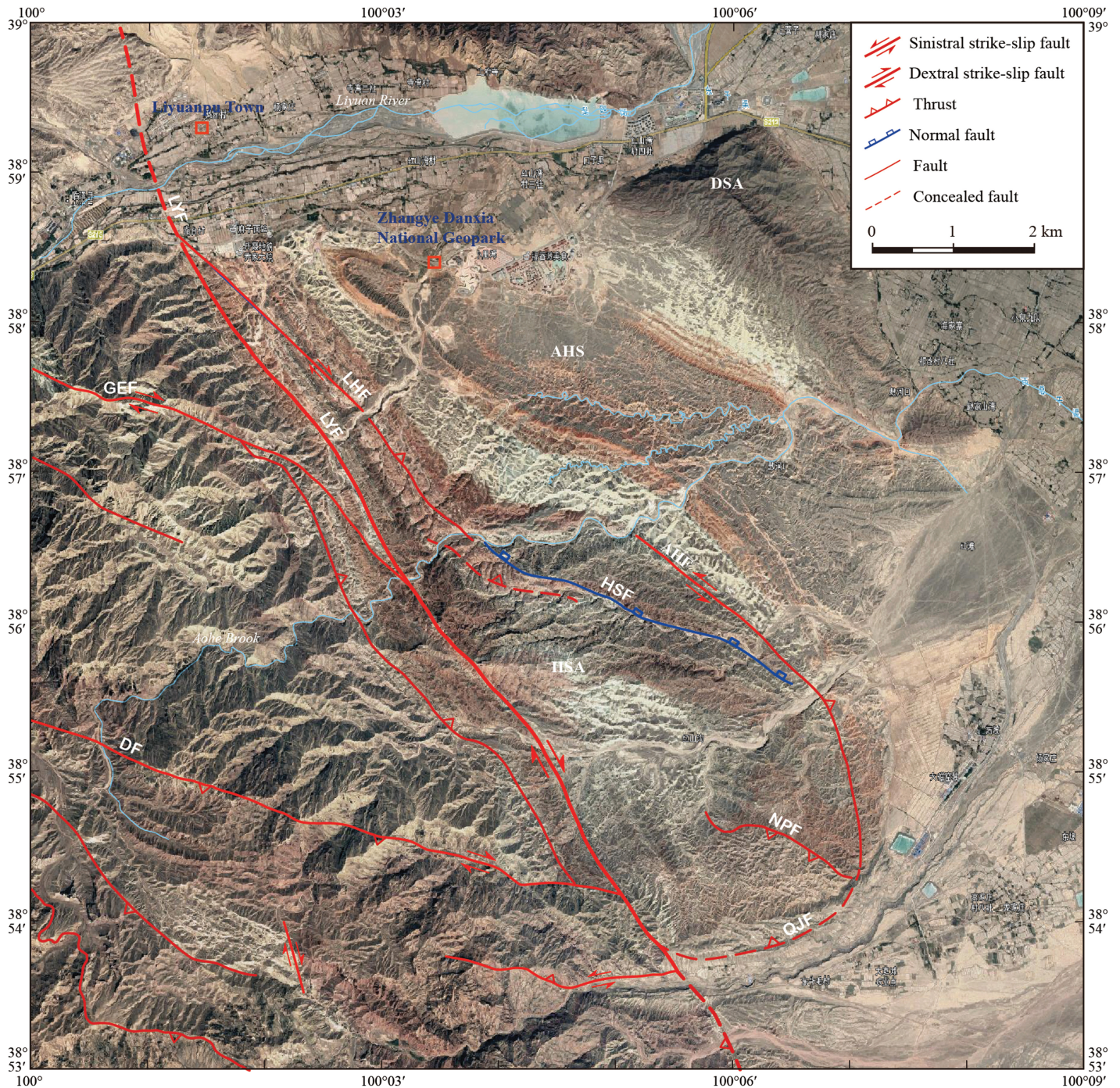


Figure 3. Geological map of the study area in the northern Qilian Shan, around the Yumu Shan, NW China, showing location of A–B sections in Figure 4. Modified from BGGP (1971, 1973), BGQP (1968), and Chen et al. (2019b). Q<sub>4</sub>—Holocene; Q<sub>3</sub>, Q<sub>2</sub>, and Q<sub>1</sub>—Upper, Middle, and Lower Pleistocene; N<sub>2</sub>—Pliocene; N<sub>1</sub>—Miocene; E—Paleogene; K<sub>1</sub>—Lower Cretaceous; J—Jurassic; T—Triassic; P—Permian; C<sub>2</sub> and C<sub>1</sub>—Upper and Lower Carboniferous; D—Devonian; S<sub>3</sub>, S<sub>2</sub>, and S<sub>1</sub>—Upper, Middle, and Lower Silurian; O<sub>3</sub>, O<sub>2</sub>, and O<sub>1</sub>—Upper, Middle, and Lower Ordovician; E—Cambrian. CMF—Changma fault; NQLF—North Qilian fault; NYMF—North Yumushan fault; SYMF—South Yumushan Fault; LSF—Longshoushan fault; LYF—Liyuanpu fault; SNF—Sunan fault; DGF—Dagengzi fault; XGF—Xiaogengzi fault; YMK—Yumu klippe. Location of Figure 4 and Figure 5A is shown as a red rectangle.





**Figure 4.** Google-Earth image of the Liyuanpu region in the intersection of the northern Qilian Shan and the southern Hexi Corridor, NW China (based on Google Earth image). LYF—Liyuanpu fault; LHF—Lanheba fault; HSF—Hongshan fault; NPF—Nianpangou fault; AHS—Aohe fault; QJF—Qijiataizi fault; GEF—Gaoerwan fault; DF—Donghe fault. AHS—Aohe syncline; DSA—Daoshan anticline; HSA—Hongshan anticlinorium.

which displays a right-separation of  $\sim 1.0$  km (Figs. 4 and 5).

The Hongshan fault extends for  $\sim 6$  km, strikes  $\sim 285^\circ$ , and dips  $60^\circ$ – $70^\circ$  to the north (Figs. 4, 5, 10C, and 10D). The fault juxtaposes the upper member of the Xinminpu Formation ( $K_1xm^a$ ) in the hanging wall over the lower

member of the same formation ( $K_1xm^{a3}$ ) in the footwall. The Nianpangou fault is a south-dipping thrust juxtaposing lower member of the Xinminpu Formation ( $K_1xm^a$ ) in the hanging wall over the upper member of the same formation ( $K_1xm^b$ ) in the footwall. The thrust strikes  $\sim N22^\circ W$  and dips  $65^\circ SW$ .

The Aohe fault is a NE-dipping oblique left-slip reverse fault (Figs. 4 and 5). It places unit  $K_1xm^{a3}$  in the hanging wall over unit  $K_1xm^{b2}$  in the footwall. The Qijiataizi fault is an inferred NW-dipping thrust, and its trace is covered by Miocene sediments ( $N_1$ ; Figs. 4 and 5).



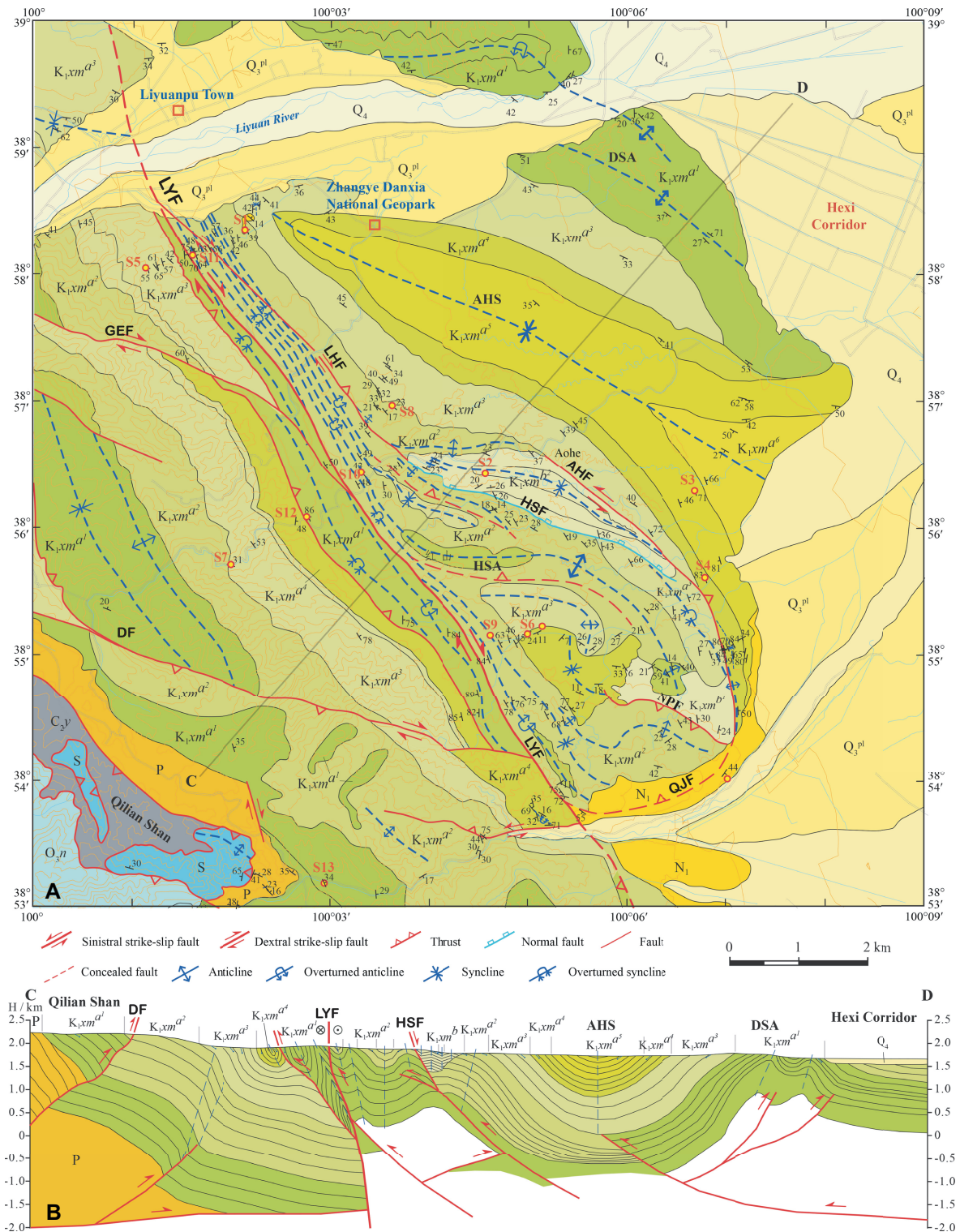


**Figure 5.** (A) Geological map of the Liyuanpu region, NW China, based on structural interpretation of Google-Earth image and field observations. Modified from Chen et al. (2019b). Q<sub>4</sub>—Holocene; Q<sub>3</sub>—Upper Pleistocene; N<sub>1</sub>—Miocene; K<sub>1</sub>—Lower Cretaceous; P—Permian; C<sub>2</sub>—Upper Carboniferous; S—Silurian; O<sub>3</sub>—Upper Ordovician. LYF—Liyuanpu fault; LHF—Lanheba fault; HSF—Hongshan fault; AHF—Aohe fault; QJF—Qijiaataizi fault; NPF—Nianpangou fault; GEF—Gaoerwan fault; DF—Donghe fault. AHS—Aoheshan syncline; DSA—Daoshan anticline; HSA—Hongshan anticlinorium. Localities of detrital zircon samples (S1–S13; see Table 1) are shown with circles. (B) Geological cross section (profile C–D) across the right lateral strike-slip Liyuanpu fault (LYF) and major folds in NE direction, showing relationships among faults and folds developed in the region.

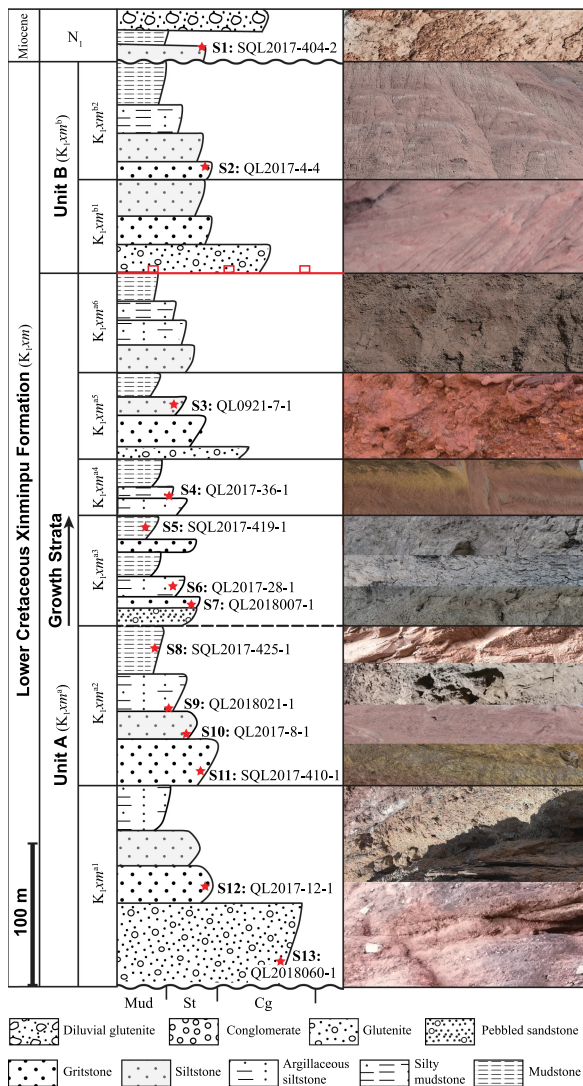


**Figure 6.** Stratigraphic framework of Lower Cretaceous Xinminpu Formation ( $K_1xm$ ) and Miocene ( $N_1$ ) strata in the Liyuanpu region, NW China. Typical lithologies are represented by photographs. Layer localities of detrital zircon samples are also shown.

## Growth Strata

Growth strata in sub-unit  $K_1xm^{a3}$  (Fig. 6) are exposed across the southeastern limb of the Hongshan anticlinorium. The growth-strata relationship is expressed by the shallowing of the fold limb dip from  $63^\circ$  stratigraphically upwards to  $7^\circ$  over a stratigraphic thickness of  $\sim 300$  m (Fig. 11). Field observations also reveal a gradual decrease in grain size from coarse-grained sandstones at the bottom of the  $K_1xm^{a3}$  to fine-grained mudstones at the top (Fig. 6). Sub-units  $K_1xm^{a1}$  and  $K_1xm^{a2}$  of the Xinminpu Formation display parallel lamination and parallel bedding, which we interpret as pre-growth deposits.

## Balanced Cross Section and Restoration

Our detailed mapping allows us to construct a balanced cross section (Fig. 5). Using the

method outlined in Bally et al. (1966) and Dahlstrom (1969) and the models of fault related folds by Suppe (1983), we restored the cross section (Fig. 12) through line balancing of a Cretaceous marker bed along section C–D in Figure 5. The restoration yields a total shortening of  $\sim 7.1$  km and a shortening strain of  $\sim 35\%$  (Figs. 12A and 12E). Note that the overlying Miocene strata are only mildly folded. Together with the observed growth-strata relationship mentioned above, the estimated shortening was mainly generated in the Cretaceous.

## DETRITAL ZIRCON GEOCHRONOLOGY

### Sample Collection and Description

We collected 12 samples from the Lower Cretaceous strata and one sample from the Miocene strata for U-Pb detrital zircon dating and

provenance analyses. The samples, numbered S1 through S13, are listed in Table 1. Sample locations on the geological map and in the stratigraphic column are shown in Figures 5A and 6, respectively. Representative petrographic views of the samples under the microscope are provided in Figure 13.

**Sample S1** is a massive and medium-coarse-grained lithic quartz sandstone from the Miocene strata ( $N_1$ ). It consists of quartz (72%), feldspar (3%), lithic clasts (15%), cementing calcite (7%) and clay minerals (2%), and pores (1%) (Fig. 13A). The sample is poorly sorted and the clasts are angular.

**Sample S2** is a massive coarse-grained gravel-bearing lithic sandstone from the middle to upper section of the upper member of the Xinminpu Formation ( $K_1xm^{b2}$ ). It is comprised of quartz (20%), potassium feldspar (20%), plagioclase (14%), lithic fragments (22%; mainly mudstone, quartzite, and chert), cement materials (10%), matrix clay minerals (4%), and gravels (8%; mainly quartzite) (Fig. 13B). It is poorly sorted and the clasts are poorly rounded.

**Sample S3** is a massive medium-grained lithic quartz sandstone from unit  $K_1xm^{a5}$ . It consists of quartz (56%), plagioclase and potassium feldspar (10%), lithic clasts (20%), calcite (8%), matrix (6%), and pores (Fig. 13C). The lithic clasts are mainly phyllite and mudstone. The sample is poorly sorted and the clasts poorly rounded.

**Sample S4** is a massive coarse-grained gravel-bearing lithic sandstone from unit  $K_1xm^{a4}$ . It is too fragile for making thin sections. Visual examination indicates its modal composition is dominated by quartz, plagioclase, potassium feldspar, and cementing calcite and clay minerals. Gravels are mainly quartzite, and lithic clasts are mudstone, quartzite, and chert.

**Sample S5** is a massive medium-coarse-grained quartz-dominated sandstone from unit  $K_1xm^{a3}$ . It is comprised of quartz (74%), feldspar (3%), and lithic clasts (12%), cementing calcites and clay minerals (10%), and pores (1%) (Fig. 13D). The lithic clasts are mainly quartzite, phyllite, and mudstones. It is moderately sorted and rounded.

**Sample S6** is a massive medium-coarse-grained quartz sandstone from unit  $K_1xm^{a3}$ . It consists of 80% quartz, 3% feldspar, 7% lithic clast, and 10% interstitial materials (Fig. 13E). It is poorly sorted and rounded. Pyrite framboids can be observed under the microscope.

**Sample S7** is a massive fine-medium-grained feldspar-rich lithic sandstone from unit  $K_1xm^{a3}$ . It is composed of 60%–65% quartz, 5%–10% plagioclase and potassium feldspar, 20%–25% lithic clasts, and 11%–20% interstitial materials (Fig. 13F). Lithic clasts are slates, phyllite,



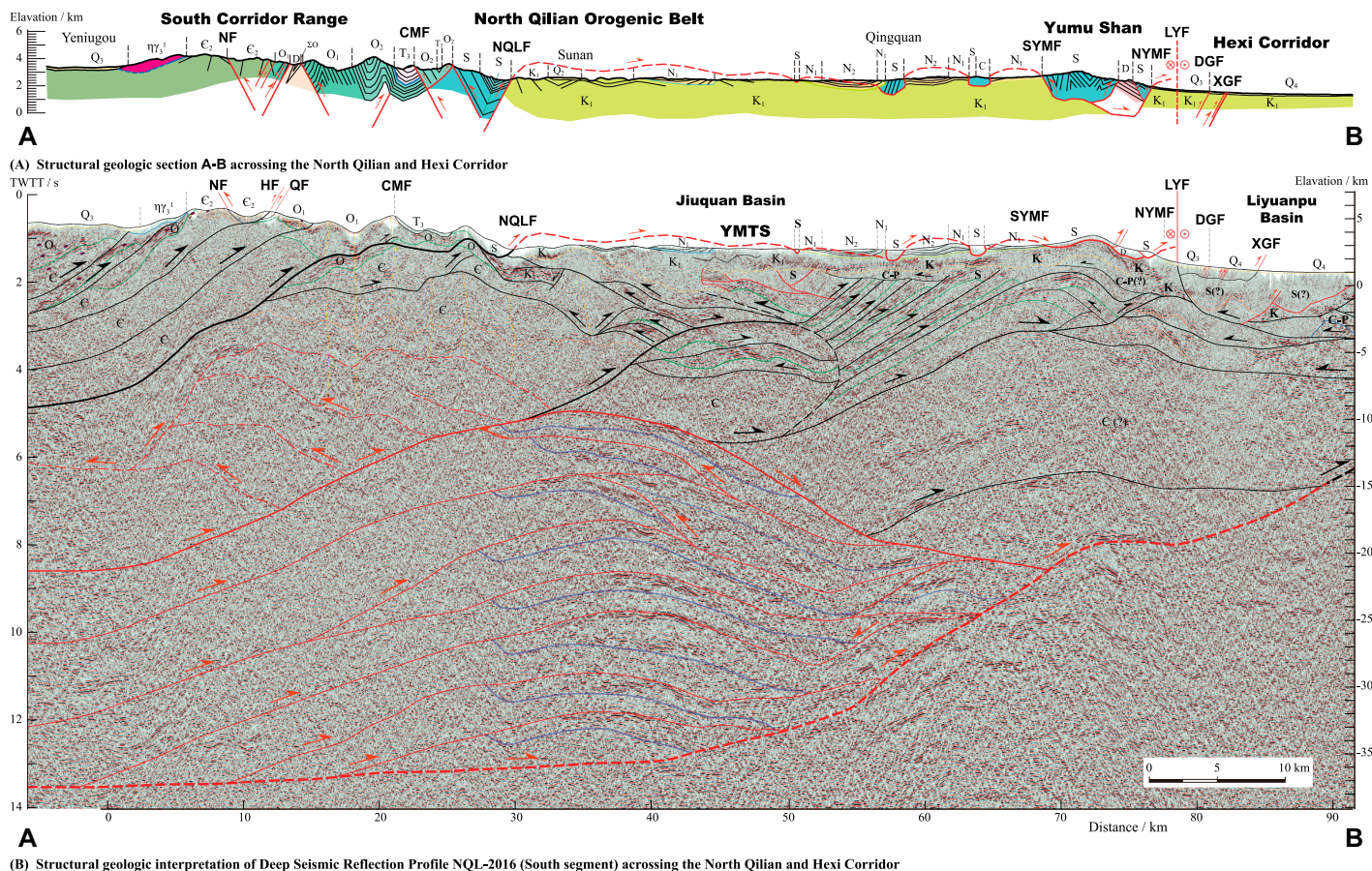


**Figure 7. (A) Geological cross section along profile A–B across the northern Qilian Shan, showing the development of the Yumu Shan thrust and nappe system (YMTS). (B) Structural interpretation of the deep seismic reflection profile NQL-2016 across the North Qilian Shan. Modified from Chen et al., 2019b. Strata systems and faults are the same as in Figures 2 and 3. See location and abbreviations in Figure 3. TWTT—two-way travel time.**

chert, siltstone, rhyolite, granite, basalt, and mica. It is poorly to moderately rounded, and poorly sorted. The sample is weakly sericitized and kaolinized.

**Sample S8** is a massive muddy micritic limestone collected from unit K<sub>1</sub>xm<sup>a2</sup>. It consists mainly of micritic calcites (83%) and iron-rich mud (12%), with minor sparry calcite (3%) and silt-sized quartz (2%) (Fig. 13G). The micritic calcite is organic-rich, whereas the sparry calcites are present along fractures 0.05–0.1 mm wide. Pyrites are distributed in the mud matrix.

**Sample S9** is a coarse-grained gravel-bearing lithic sandstone from unit K<sub>1</sub>xm<sup>a2</sup>. It consists of 55%–60% quartz, 1%–5% plagioclase and potassium feldspars, 25%–30% lithic clasts, 5%–10% gravel-sized debris, and 10%–15% calcite cements and clay-rich interstitial matrix materials (Fig. 13H). Lithic clasts are slates, phyllite, chert, rhyolite, andesite, and altered basalt. Gravel-sized clasts are mainly metamorphosed silty sandstone. The sample is weakly sericitized and kaolinized.

**Sample S10** is a massive medium-grained lithic sandstone from unit K<sub>1</sub>xm<sup>a2</sup>. It consists of 32% quartz, 8% plagioclase, 50% lithic clasts, 4% micritic cements, and 6% clay-rich matrix (Fig. 13I). It is poorly sorted and rounded. Lithic clasts are mainly silty mudstone and rare chert.

**Sample S11** is a massive silty mudstone collected from unit K<sub>1xm</sub><sup>a2</sup>. It consists of 92% clay minerals, 3% sericites, and 5% silt-sized quartz grains (Fig. 13J).

**Sample S12** is a massive medium-fine-grained lithic feldspathic sandstone from unit K<sub>1</sub>xm<sup>a1</sup>. It consists of 40% quartz, 23% plagioclase, 24% lithic clasts, 6% cements, 6% matrix clay minerals, and 1% detrital biotite, muscovite, and secondary minerals (Fig. 13 K). It is poorly to moderately rounded and poorly sorted. Sparry calcites occur as fracture fills. Lithic clasts are mainly mudstone fragments.

**Sample S13** is a massive coarse-grained lithic quartz sandstone collected from unit K<sub>1</sub>xm<sup>a1</sup>. It consists of 80%–85% quartz, 1%–5% potassium feldspar, 15%–20% lithic clasts, 2%–8% inter-

stitial materials (Fig. 13L), and a small number of gravel-sized clasts (2.0–2.5 mm). Lithic clasts are rhyolite, tuff, slate, quartzite, chert, and sparry limestone. Gravel-sized clasts are rhyolite and quartzite. The interstitial materials are fine-grained clay minerals and calcite cements. It is moderately rounded and well sorted. The sample is weakly kaolinized.

## Sample Preparation and Analytical Methods

Detrital zircons were extracted from the samples through roller crushing and grinding, heavy mineral separation and hand picking under binocular microscope. They were mounted in epoxy resin, solidified, and then polished and ground to approximately half of the thickness until their cores were fully exposed. Zircons were examined both in reflected and transmitted light, and imaged by cathodoluminescence (CL) (Fig. 14), to characterize their internal microstructures and to target sites.



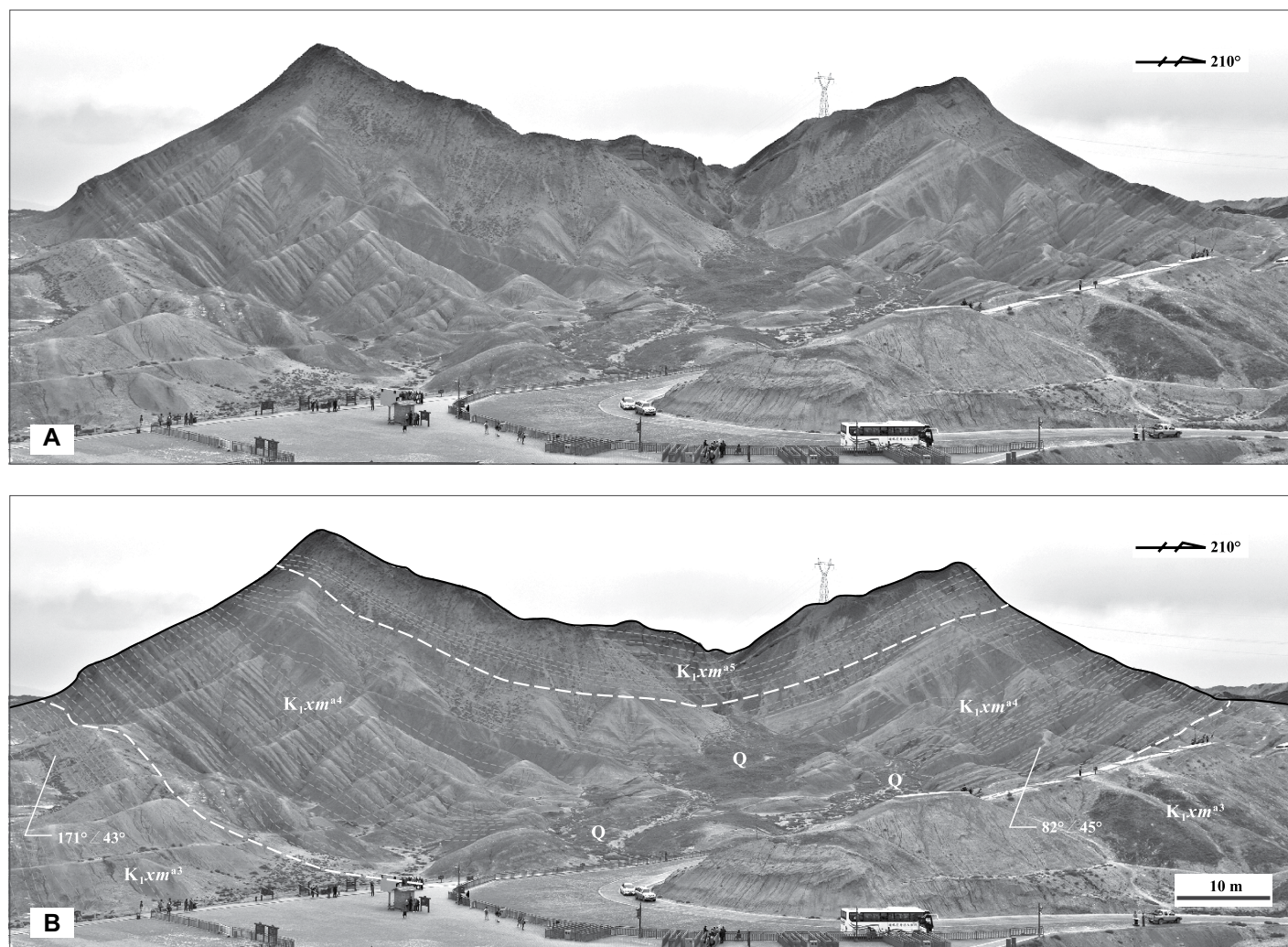


**Figure 8.** Field photographs of the Aoheshan syncline (AHS) developed in Unit A of the Lower Cretaceous. (A and B) are original photograph and interpreted structure, respectively. Taken at the position of 38°58'27.9"N and 100°2'28.6"E, near a main gate of the Zhangye Danxia National Geopark, NW China.

Zircon U-Pb isotope analyses were conducted by laser ablation–multicollector–inductively coupled plasma–mass spectrometry (LA-MC-ICP-MS) with Neptune X-Series II multi-receiving plasma mass spectrometer (ThermoFisher), at the Tianjin Geological Survey Center, China Geological Survey. The analyses involve zircon ablation with a New Wave FX laser (operating at a wavelength of 193 nm) using a spot diameter of 35  $\mu\text{m}$  (Hu et al., 2015a). Details of the instrument parameters and analytical procedures are provided by Li et al. (2009). Zircon standard 91500 and standard glass NIST610 were used as external standards for fractionation correction of U-Pb isotopes and trace elements, respectively. Each set of time-resolved data consists of  $\sim 20$ –30 s of blank analysis and 50 s of sample analysis. Data processing, which involved selections of

sample and blank signals, instrument sensitivity drift corrections, and calculations of element concentrations, and U-Pb isotopic ratios, was completed using software ICPMSDataCal (Liu et al., 2008). ISOPLOT/Ex\_ver3 (Ludwig, 2003) was used for age calculation.

#### U-Pb Detrital Zircon Ages

CL images show that the shape and size of the zircons are variable (Fig. 14). Most of the zircons are rounded, typical for detrital zircon grains in sedimentary rocks. A total of 90–110 zircon grains were selected randomly from each sample, and only analyses of 90%–100% concordant were included in the statistical analyses for age spectra. U-Pb ages were calculated using  $^{206}\text{Pb}/^{238}\text{U}$  ratios for zircons  $\leq 1000$  Ma and  $^{207}\text{Pb}/^{206}\text{Pb}$  ratio for zircons  $> 1000$  Ma. The

analytical data are reported in Supplementary Tables S1–S13<sup>1</sup>, shown on U-Pb concordia diagrams (Fig. 15) and age spectra (Fig. 16), and summarized in Table 1.

**Sample S1.** Detrital zircons are prismatic to sub-rounded shaped with 50–180  $\mu\text{m}$  in size. A total of 103 grains were analyzed, with 12 discordant ages (concordant  $< 90\%$ ) excluded. Their Th/U ratios range from 0.03 to 3.98. U-Pb ages are grouped around the main peak at ca. 265 Ma, and minor peaks at ca. 427 Ma and ca. 367 Ma (Figs. 15A and 16A). The youngest zircon age is  $257 \pm 3$  Ma.

<sup>1</sup>Supplemental Material. U-Pb isotope dating results for the detrital zircons from sample S1–S13. Please visit <https://doi.org/10.1130/GSAB.S.14489154> to access the supplemental material, and contact [editing@geosociety.org](mailto:editing@geosociety.org) with any questions.



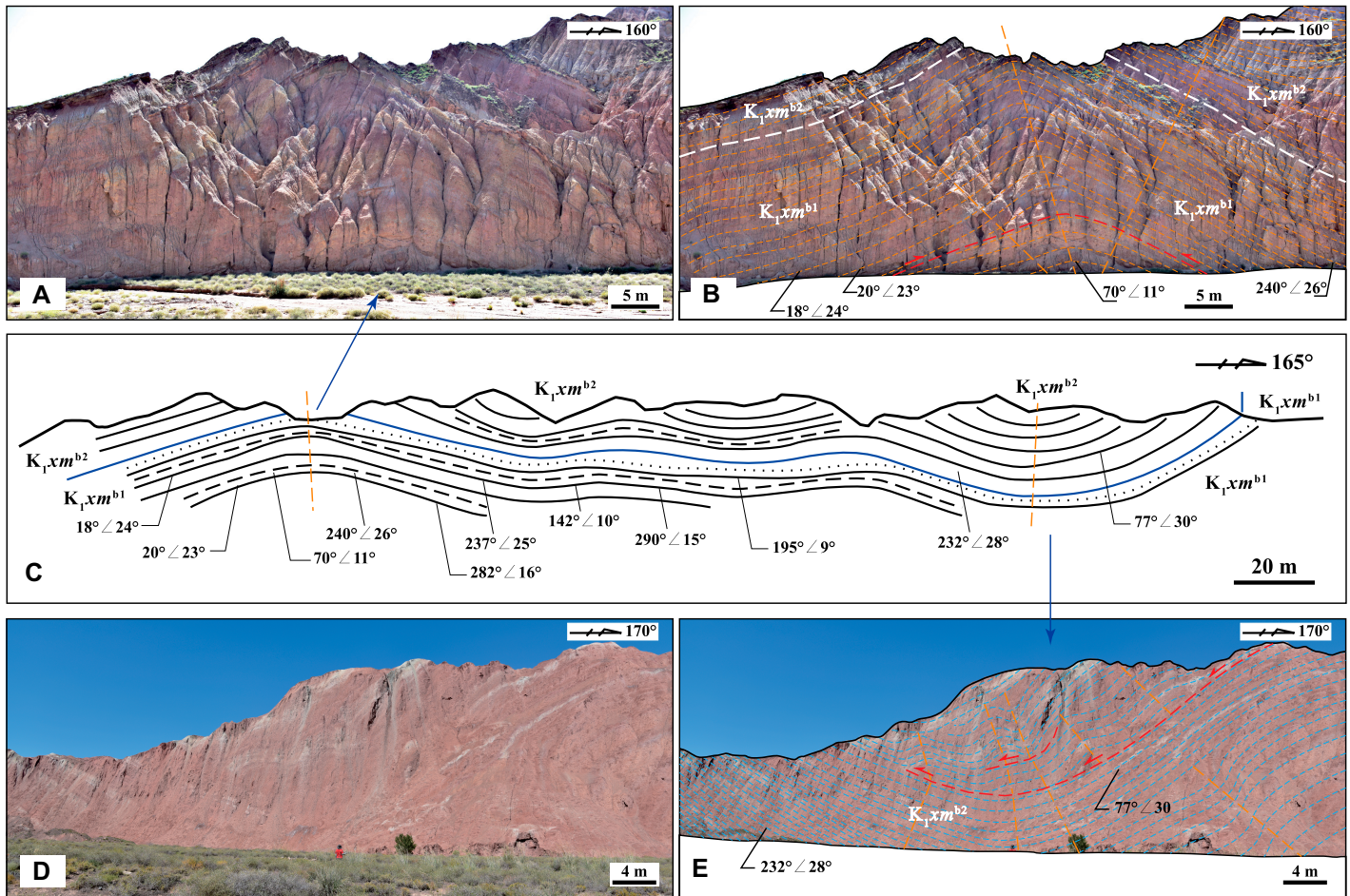


**Figure 9.** Folds developed in Unit B of the Lower Cretaceous, north to the Hongshan Anticlinorium (HSA), Liyuanpu region, NW China. (A) Original and (B) interpreted photographs of the anticline in the north, and (D) original and (E) interpreted photographs of the syncline in the south. Relationship between the anticline and syncline are shown in panel C. Location is at 38°56'30.6"N and 100°4'6.4"E.

**Sample S2.** Detrital zircons are sub-rounded and 40–140  $\mu\text{m}$  in size. 92 spots were analyzed, and 11 points (<90% concordant) were excluded. Th/U values range from 0.06 to 5.85. The U-Pb ages are clustered mostly at ca. 408 Ma and ca. 280 Ma, with minor clusters at ca. 807 Ma, ca. 932 Ma, and ca. 1884 Ma. The youngest age is  $258 \pm 3$  Ma (Figs. 15B and 16B).

**Sample S3.** Detrital zircons are sub-rounded and 60–190  $\mu\text{m}$  in size. 109 spots were analyzed, and one discordant point (<90% concordant) was excluded. The Th/U values range from 0.03 to 1.67. The main age clusters are at ca. 274 Ma and ca. 413 Ma, while two minor clusters are at ca. 1744 and ca. 2470 Ma. The youngest age is  $239 \pm 3$  Ma (Figs. 15C and 16C).

**Sample S4.** Detrital zircons are sub-rounded and 75–180  $\mu\text{m}$  in size. 98 spots were analyzed, and two spots were excluded because they are <90% concordant. The Th/U values are 0.08–1.77. The ages are mainly clustered at ca. 266 Ma and ca. 442 Ma, with minor clusters at

ca. 1864 and ca. 2582 Ma. The youngest age is  $246 \pm 2$  Ma (Figs. 15D and 16D).

**Sample S5.** Detrital zircons are long columnar to sub-rounded, with 65–175  $\mu\text{m}$  in size. 99 spots were analyzed and 15 discordant points (<90% concordant) were excluded. The Th/U values range from 0.12 to 3.78. U-Pb ages are mainly clustered at ca. 402 Ma and ca. 279 Ma, with a minor cluster centered at ca. 1946 Ma. The youngest zircon age is  $241 \pm 3$  Ma (Figs. 15E and 16E).

**Sample S6.** Detrital zircons are short columnar to sub-rounded and 50–180  $\mu\text{m}$  in size. 99 spots were analyzed and none were excluded. The Th/U values are 0.09–1.91. The main age clusters are at ca. 286 Ma and ca. 473 Ma, and minor clusters are at ca. 981 and ca. 1870 Ma, respectively. The youngest age is  $268 \pm 3$  Ma (Figs. 15F and 16F).

**Sample S7.** Detrital zircons are prismatic to sub-rounded and 65–190  $\mu\text{m}$  in size. 101 spots were analyzed, with 10 spots excluded as <90%

concordant. The Th/U values are 0.18–1.70. The main age clusters are at ca. 277 Ma and ca. 432 Ma, and minor ones are at ca. 1846 and ca. 2488 Ma. The youngest age is  $237 \pm 2$  Ma (Figs. 15G and 16G).

**Sample S8.** Detrital zircons are short columnar to sub-rounded and 45–135  $\mu\text{m}$  in size. 98 spots were analyzed and 13 analyses were excluded because of <90% concordant. Their Th/U values are 0.002–2.77. The main age clusters are at ca. 438 Ma and ca. 277 Ma, and minor clusters are at ca. 752 Ma, ca. 957 Ma, and ca. 2486 Ma. The youngest age is  $233 \pm 2$  Ma (Figs. 15H and 16H).

**Sample S9.** Detrital zircons are prismatic to sub-rounded and 75–245  $\mu\text{m}$  in size. A total of 101 spots were analyzed, among which seven spots were excluded because of <90% concordant. Their Th/U values are 0.17–2.42. The main age clusters are at ca. 280 Ma and ca. 427 Ma, and minor age clusters are centered at ca. 931 and ca. 1841 Ma. The youngest age is  $233 \pm 2$  Ma (Figs. 15I and 16I).



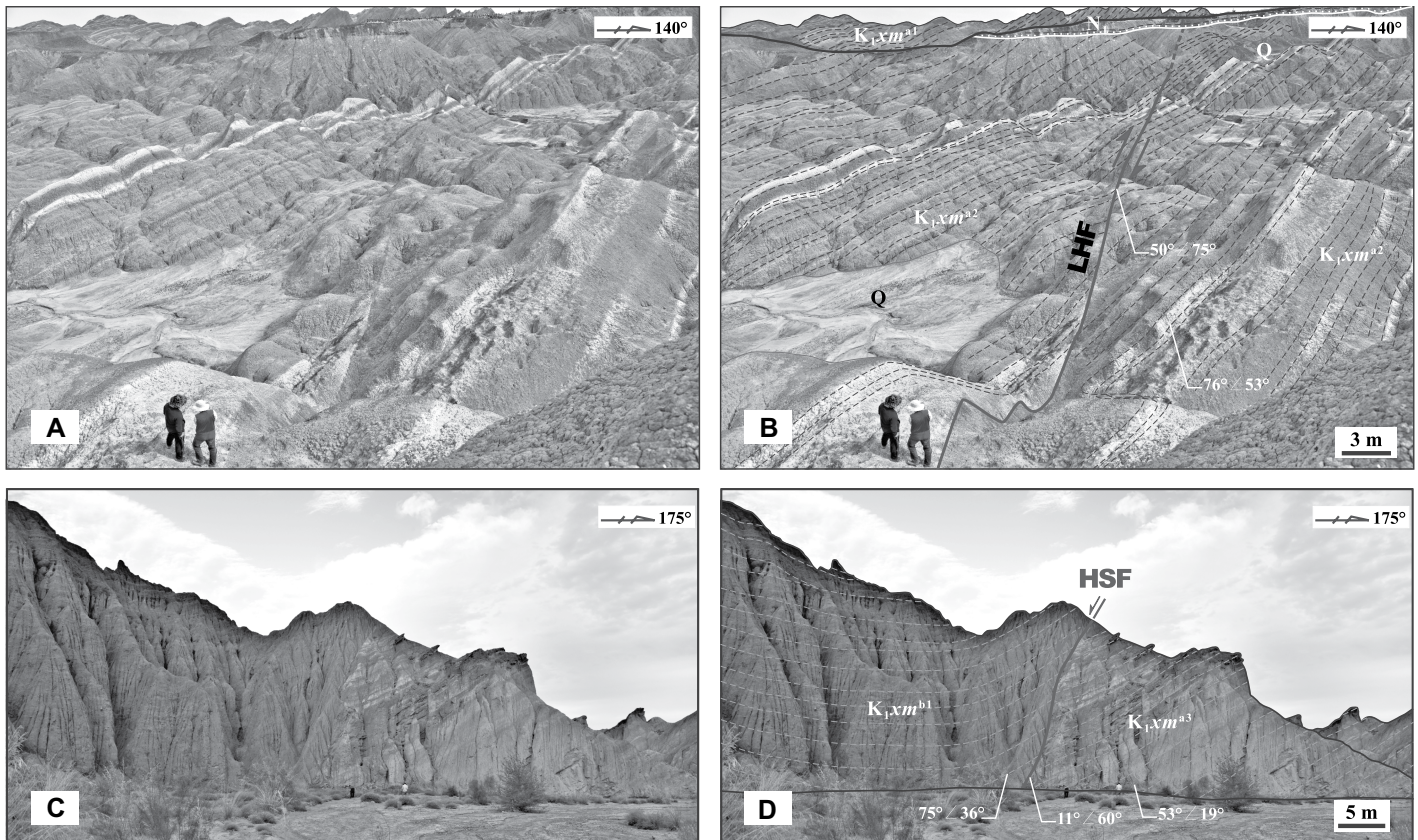


**Figure 10.** Field photographs of typical faults developed in the Liyuanpu region, NW China. (A) Original and (B) interpreted photograph of the Lanheba fault (LHF), which branches off the major right-lateral strike-slip Liyuanpu fault (LYF) at a small angle (Fig. 5) (photo taken at  $38^{\circ}58'10.5''\text{N}$  and  $100^{\circ}1'42.9''\text{E}$ ). The strike-slip fault system is unconformably covered by shallowly dipping Miocene sedimentary rocks ( $N_1$ ). (C) Original and (D) interpreted photographs of the Hongshan fault (HSF), which is a steep north-dipping normal fault that cuts Lower Cretaceous rocks (taken at  $38^{\circ}55'54.8''\text{N}$  and  $100^{\circ}5'42.6''\text{E}$ ).

**Sample S10.** Detrital zircons are long columnar to sub-rounded and  $70\text{--}200\ \mu\text{m}$  in size. 89 spots were analyzed, of which three were excluded. The Th/U values are  $0.04\text{--}3.90$ . The main age clusters are at ca. 468 Ma and ca. 279 Ma, and the minor age clusters are at ca. 807 Ma, ca. 967 Ma, ca. 2011 Ma, and ca. 2505 Ma. The youngest age is  $258 \pm 3\ \text{Ma}$  (Figs. 15J and 16J).

**Sample S11.** Detrital zircons are long columnar to sub-rounded and  $45\text{--}180\ \mu\text{m}$  in size. 101 spots were analyzed, with 12 spots excluded. The Th/U values are  $0.05\text{--}13.43$ . The main age clusters are at ca. 435 Ma and ca. 297 Ma, and a minor cluster at ca. 974 Ma. The youngest age is  $255 \pm 3\ \text{Ma}$  (Figs. 15K and 16K).

**Sample S12.** Detrital zircons are long columnar to sub-rounded and  $40\text{--}170\ \mu\text{m}$  in size. A total of 104 spots were analyzed, with two spots excluded. The Th/U values are  $0.04\text{--}1.63$ . The main age clusters are at ca. 304 Ma, ca. 274 Ma, ca. 343 Ma, and ca. 442 Ma, and a minor cluster at ca. 1872 Ma. The youngest zircon age is  $244 \pm 2\ \text{Ma}$  (Figs. 15L and 16L).

**Sample S13.** Detrital zircons are prismatic to sub-rounded and  $70\text{--}190\ \mu\text{m}$  in size. A total of 100 spots were analyzed, and eight discordant analyses were excluded. Their Th/U values are  $0.12\text{--}2.24$ . The main age clusters are at ca. 291 Ma and ca. 423 Ma, and minor clusters are at ca. 1775 Ma, ca. 1933 Ma, and ca. 2534 Ma. The youngest zircon age is  $246 \pm 3\ \text{Ma}$  (Figs. 15M and 16M).

## DISCUSSION

The new geologic map created in this research provides the tightly constrained field relationship between the formation of folds and the development of growth strata in the Cretaceous unit. The newly acquired U-Pb detrital zircon ages allow a detailed provenance analysis of the Cretaceous and Miocene strata from which the samples were collected. Below, we discuss the implications of our findings.

Previous work shows that the early Paleozoic Qilian orogen in northern Tibet was reactivated during the Cenozoic Indo-Asian collision by

the development of thrusting and strike-slip faulting (Zuza et al., 2016, 2018, 2019; Li et al., 2021). Deformation recorded in the Cretaceous strata in the northern Tibetan plateau and its foreland region may have occurred during the onset of the Indo-Asian collision or even before (Frost et al., 1995; Dupont-Nivet et al., 2004). We propose a three-stage model for the tectonic deformation of the study area in the Cretaceous and Cenozoic based on the following interpretations. (1) The angular unconformity between the Miocene and the Cretaceous strata (Figs. 7 and 11) implies a protracted erosion and peneplanation process from the Late Cretaceous (i.e., after the deposition of the Lower Cretaceous strata) to the end of Paleogene when the Miocene strata were deposited. In this interpretation, folding in the Lower Cretaceous strata occurred prior to the interpreted peneplanation event. (2) The occurrence of growth strata in unit  $K_1xm^{a3}$  indicates folding during the deposition of the Early Cretaceous in the study area. (3) The local presence of the upper member of the Xinminpu Form ( $K_1xm^b$ ), and drastic



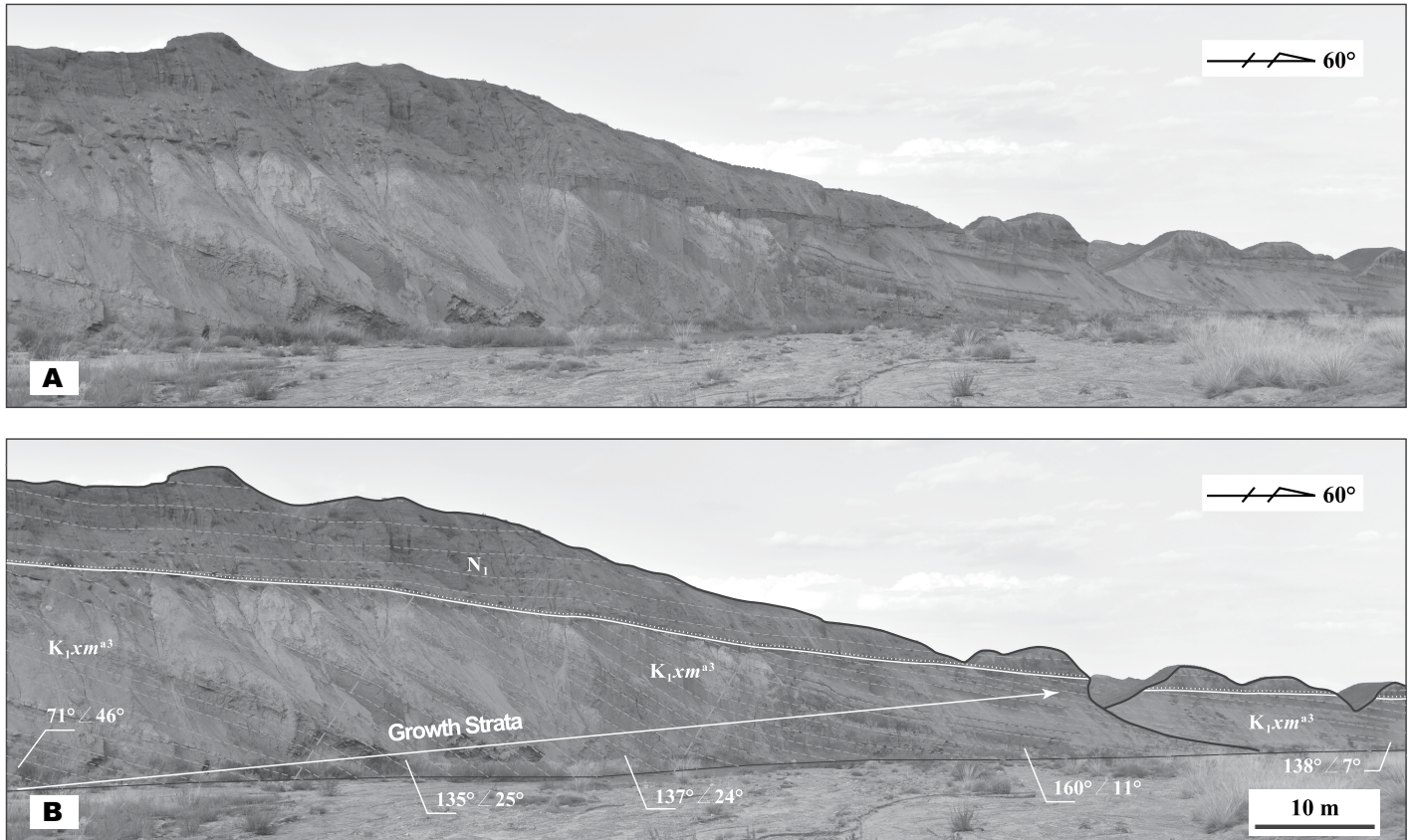


**Figure 11.** Growth strata developed in Unit A of the Lower Cretaceous Xinminpu Formation, in the south limb of the Hongshan Anticlinorium (taken at 38°55'12.2"N and 100°5'8.9"E), Liyuanpu region, NW China. (A and B) are original photograph and interpreted structure, respectively. The growth strata are covered by Miocene sedimentary rocks ( $N_1$ ) with gentle dips.

contrast in the tightness of folds in the Cretaceous and Miocene strata requires a significant shortening event in the study area prior to the Miocene, consistent with our growth-strata relationship. (4) The occurrence of normal faulting at the time between the deposition of the upper and lower member of the Xinminpu Formation (Figs. 10C and 10D) suggests an extensional origin for the deposition of the upper member. The three-stage tectonic model is shown in Figure 12 and detailed below.

### Stage 1. Early Cretaceous Folding and Thrust faulting

We infer that the sub-unit  $K_{1xm}^{a3}$  (Fig. 6) as a set of growth strata were deposited in the piedmont depression as a response to the development of the Daoshan anticline and the Hongshan anticlinorium during the earlier Early Cretaceous. Major folds, such as the Daoshan anticline, the Aoheshan syncline (Fig. 8), and the Hongshan anticline were created during NE-SW compression during the development of the growth strata (Fig. 11). Coeval with this folding was the development of the Yumushan

thrust and nappe system and Yumushan klippe documented by an earlier study (Figs. 3 and 7; Chen et al., 2019b). Possible thrust-induced basins in the Early Cretaceous may include the Pingshanhu basin deposited prior to ca. 129 Ma (Shao et al., 2019) north to the Longshou Shan thrust.

We suggest that the Early Cretaceous compressional event in the study area of northernmost Tibet and its foreland occurred during the final closure of the Bangong-Nujiang ocean and continued convergence between the Lhasa and Qiangtang terranes (Kazmin, 1991; Kapp et al., 2003; Volkmer et al., 2007; Metcalfe, 2013; Li et al., 2019c; Tang et al., 2020; Zhao et al., 2017; Ma et al., 2018; Lai et al., 2019; Cao et al., 2019; Chen et al., 2020; Li et al., 2020b). Li et al. (2019b) suggested the final closure of the Bangong-Nujiang ocean and the initial collision between the Lhasa and the Qiangtang terranes occurred at 152–150 Ma. Accelerated exhumation and crustal thickening was initiated at ca. 150 Ma in the southern Qiangtang terrane (Zhao et al., 2017, 2020). Paleomagnetic studies indicate that the Lhasa-Qiangtang collision may have occurred at ca. 145 Ma (Ma et al.,

2018). Early Cretaceous basin evolution in the northern Lhasa terrane implies the timing of the initial Lhasa-Qiangtang collision at ca. 122 Ma (Lai et al., 2019) or before ca. 119 Ma (Li et al., 2020b). The above timing is consistent with the age of compressional deformation in our study area (Fig. 17A).

### Stage 2A. Post-folding Early Cretaceous Normal Faulting

Our field mapping and field observations show that the WNW-striking Hongshan fault is a normal fault developed during the later stage of the Early Cretaceous. Its orientation indicates approximately N-S extension. The strike of this fault is generally parallel to the trend of the other known Cretaceous extensional basins in the Qilian Shan foreland (i.e., the Hexi Corridor), which include the Early Cretaceous grabens and half-grabens in the Cretaceous Jiuquan, Minle, Chaoshui, and Pingshanhu basins (Vincent and Allen, 1999; Li, 2003; Chen et al., 2014a; Cheng et al., 2019b; Shao et al., 2019). Detrital zircon U-Pb dating revealed the formation of grabens and

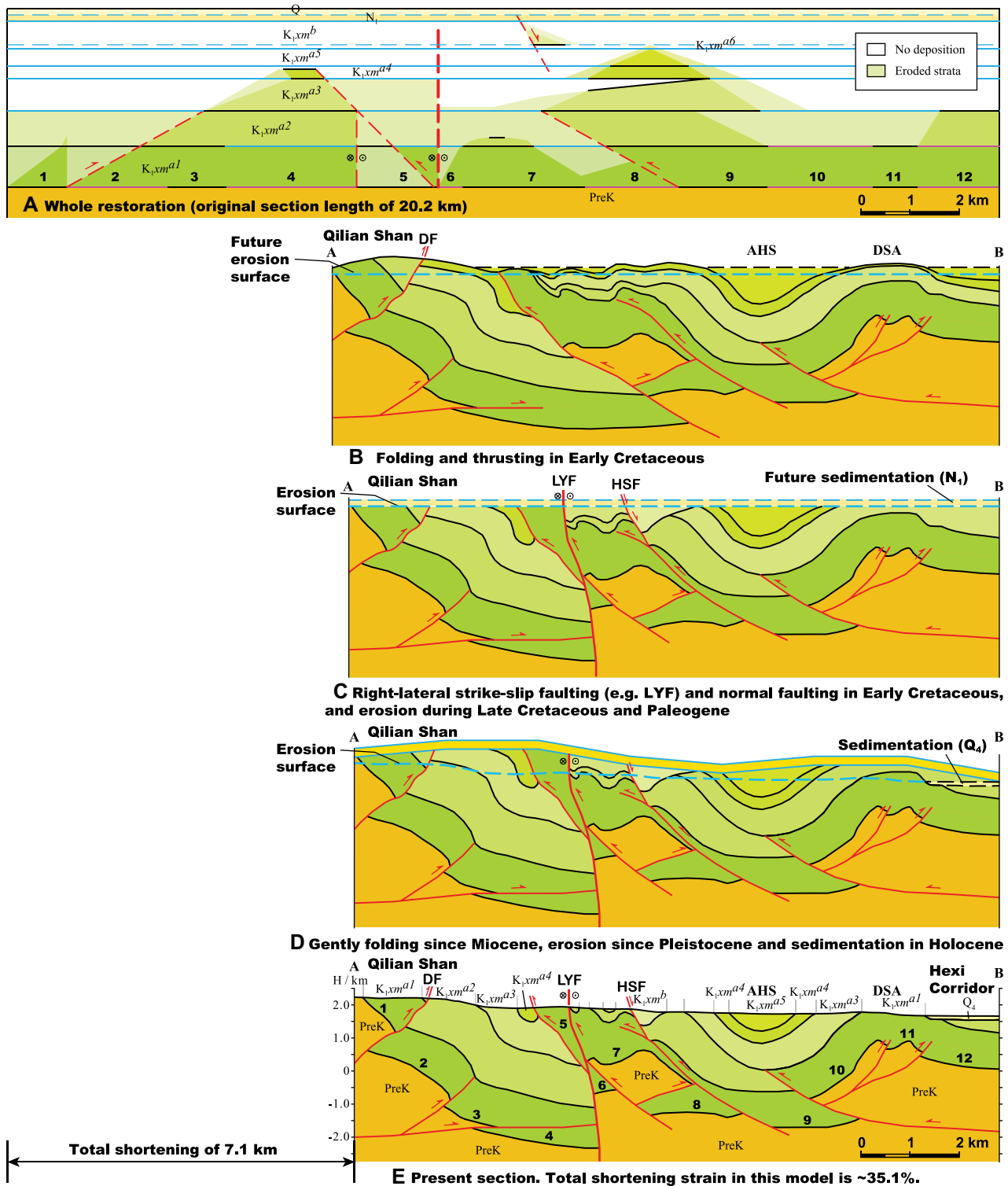


**Figure 12.** Restoration and kinematic reconstruction of the cross section shown in Figure 5 (see Fig. 5 for abbreviations). The strata have been divided into Pre-Cretaceous (PreK), Units A and B of the Lower Cretaceous Xinminpu Formation ( $K_{1xm}^a$ – $K_{1xm}^b$ ), Miocene ( $N_1$ ), and Holocene ( $Q_4$ ). (A) Undeformed restoration of the balanced section (see location in Fig. 5A), with original section length of 20.2 km. (B) Development of folds and thrusts in the earlier stage of Early Cretaceous. (C) Development of right-lateral strike-slip faults (e.g., LYF) and normal faults in the later stage of Early Cretaceous, followed by erosion during the Late Cretaceous and Paleogene. (D) Gently folding since Miocene, followed by erosion since Pleistocene and sedimentation in Holocene. (E) Present-day deformed-state cross section as shown in Figure 5. Total shortening strain in this model is 7.1 km or ~35.1% strain.



TABLE 1. SUMMARY OF DETRITAL ZIRCON U-Pb DATING OF LOWER CRETACEOUS AND MIOCENE SEDIMENTARY ROCK SAMPLES FROM THE LIYUANPU AREA, NW CHINA

No.	Sample no.	Stratum layer	GPS position		Elevation (m)	Lithology	Mineral assemblage	Peak ages (Ma)	Youngest age (Ma)
			Lat (°N)	Long (°E)					
S1	SQL2017-404-2	N <sub>1</sub>	38°58'24.0"	100°2'17.9"	1737	Lithic quartz sandstone	Qz + Lf + Fs	265, 367, 427	257
S2	QL2017-4-4	K <sub>1</sub> xm <sup>b2</sup>	38°56'27.8"	100°4'43.1"	1736	Gravel-bearing lithic sandstone	Qz + Lf + Kfs + Pl	280, 408, 807, 932, 1884	258
S3	QL0921-7-1	K <sub>1</sub> xm <sup>a5</sup>	38°56'19.7"	100°6'49.9"	1712	Lithic quartz sandstone	Qz + Lf + Pl	274, 413, 1744, 2470	239
S4	QL2017-36-1	K <sub>1</sub> xm <sup>a4</sup>	38°55'38.7"	100°6'56.7"	1698	Gravel-bearing lithic sandstone	Qz + Lf + Fs	266, 442, 1864, 2582	246
S5	SQL2017-419-1	K <sub>1</sub> xm <sup>a3</sup>	38°58'5.0"	100°1'17.2"	1795	Lithic quartz sandstone	Qz + Lf + Fs	279, 402, 1946	241
S6	QL2017-28-1	K <sub>1</sub> xm <sup>a3</sup>	38°55'12.2"	100°5'8.9"	1784	Lithic quartz sandstone	Qz + Lf + Fs	286, 473, 981, 1870	268
S7	QL2018007-1	K <sub>1</sub> xm <sup>a3</sup>	38°55'45.22"	100°2'5.4"	1808	Lithic sandstone	Qz + Lf + Fs	277, 432, 1846, 2488	237
S8	SQL2017-425-1	K <sub>1</sub> xm <sup>a2</sup>	38°57'00"	100°3'46.4"	1745	Micritic limestone	Mi + la	292, 438, 752, 957, 2486	233
S9	QL2018021-1	K <sub>1</sub> xm <sup>a2</sup>	38°55'8.67"	100°4'46.91"	1730	Gravel-bearing lithic sandstone	Qz + Lf + Fs	280, 427, 931, 1841	233
S10	QL2017-8-1	K <sub>1</sub> xm <sup>a2</sup>	38°56'28.3"	100°3'28"	1797	Lithic sandstone	Qz + Lf + Pl	279, 468, 807, 967, 2011, 2505	258
S11	SQL2017-410-1	K <sub>1</sub> xm <sup>a2</sup>	38°58'11.5"	100°1'46.1"	1749	Silty mudstone	Cl + Qz + Ms	297, 435, 974	255
S12	QL2017-12-1	K <sub>1</sub> xm <sup>a1</sup>	38°56'7.4"	100°2'55.1"	1823	Lithic feldspathic sandstone	Qz + Lf + Pl	274, 304, 343, 442, 1872	244
S13	QL2018060-1	K <sub>1</sub> xm <sup>a1</sup>	38°53'13.84"	100°2'52.23"	1927	Lithic quartz sandstone	Qz + Lf + Fs	291, 423, 1775, 1933, 2534	246

Notes: Qz—quartz; Fs—feldspar; Lf—lithic fragment; Mi—micrite; la—Iron argillaceous; Kfs—K-feldspar; Pl—plagioclase; Cl—clay mineral; Ms—muscovite.

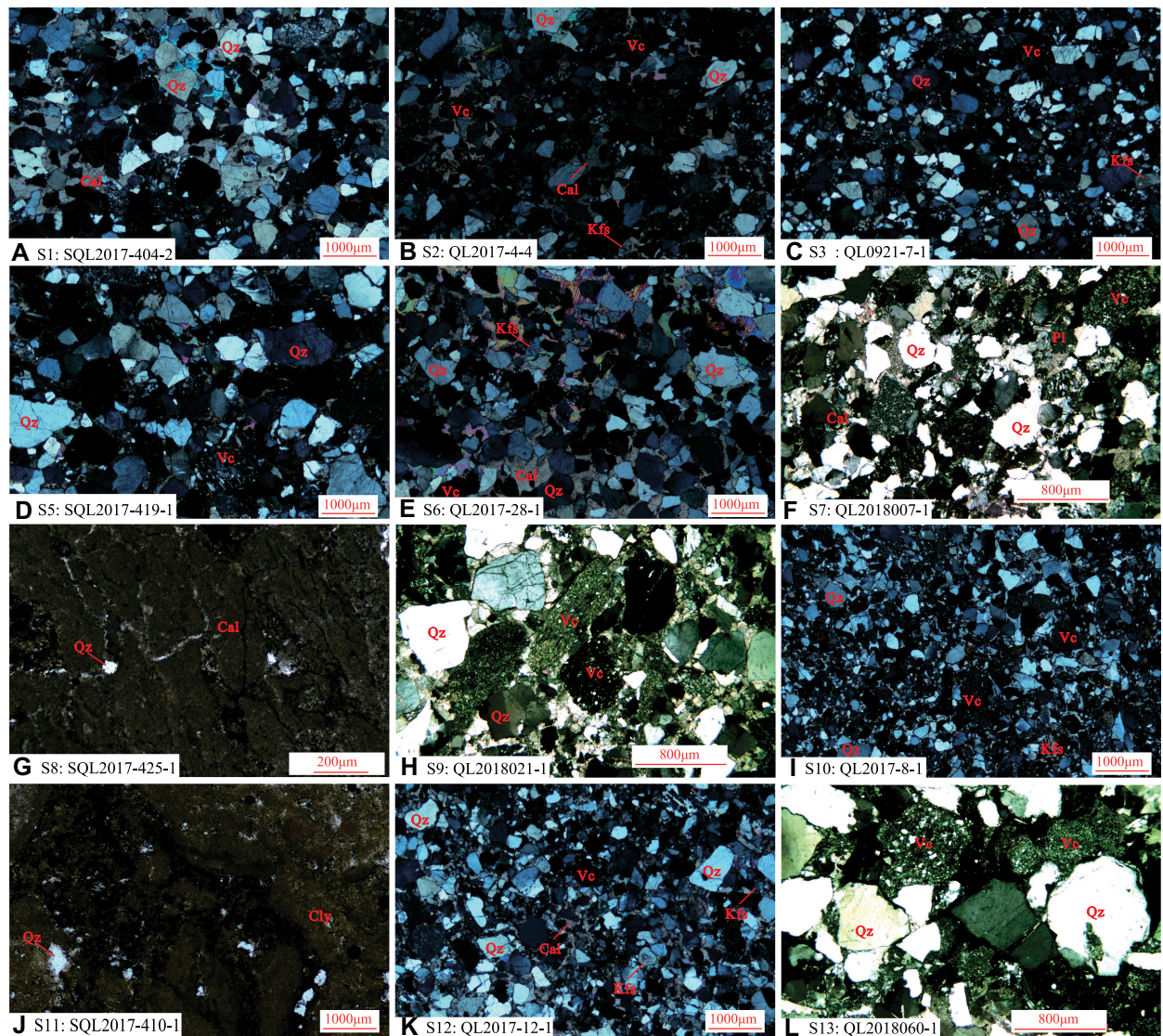
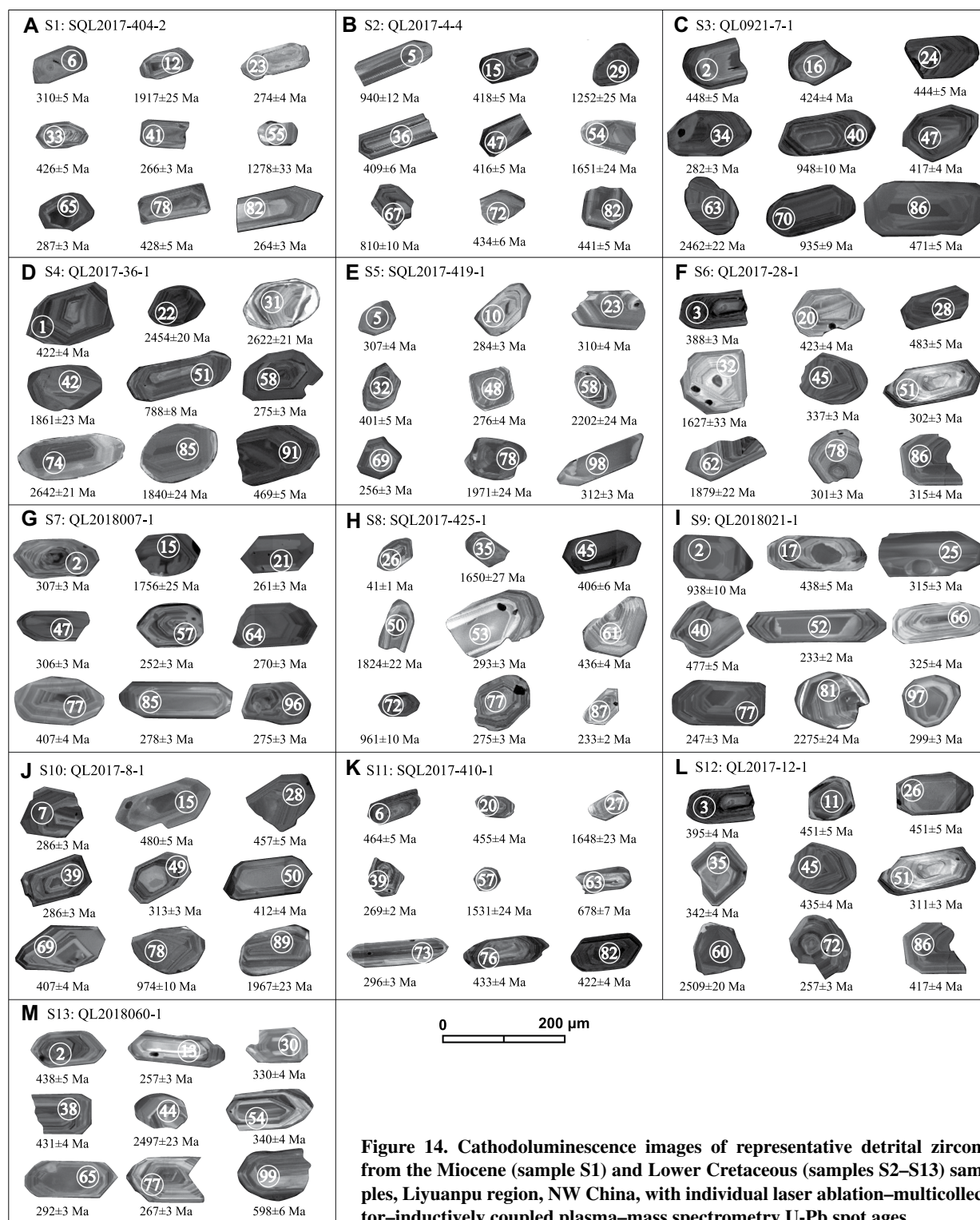


Figure 13. Photomicrographs of sedimentary rocks from Miocene (A) and Lower Cretaceous (B–L) in the Liyuanpu region, NW China. (A) S1—SQL2017-404-2; (B) S2—QL2017-4-4; (C) S3—QL0921-7-1; (D) S5—SQL2017-419-1; (E) S6—QL2017-28-1; (F) S7—QL2018007-1; (G) S8—SQL2017-425-1; (H) S9—QL2018021-1; (I) S10—QL2017-8-1; (J) S11—SQL2017-410-1; (K) S12—QL2017-12-1; (L) S13—QL2018060-1. Except plane polarized light for samples S8 and S11, the others are all under crossed polarized light. Qz—Quartz; Cal—Calcite; Kfs—K-feldspar; Pl—Plagioclase; Cly—Clay minerals; Vc—Volcanic debris.





**Figure 14.** Cathodoluminescence images of representative detrital zircons from the Miocene (sample S1) and Lower Cretaceous (samples S2–S13) samples, Liyuanpu region, NW China, with individual laser ablation–multicollector–inductively coupled plasma–mass spectrometry U–Pb spot ages.

half-grabens in the Pingshanhu basin was ongoing at ca. 129 Ma (Shao et al., 2019). The Yagan metamorphic core complex north of our study area occurred at 129–126 Ma (Zheng and Zhang, 1994). Continental basalts with ages of 120–102 Ma indicate Early Cretaceous

extension in the Hexi Corridor and Alxa block (Tang et al., 2012; Hui et al., 2020). The Cretaceous extensional event may explain earlier observed apatite fission-track cooling ages at  $124 \pm 11$  Ma from Triassic granite samples in the Qilian Shan (Qi et al., 2016; Li et al.,

2019a, 2020a). Finally, an extensional event at ca. 100 Ma was reported in the eastern Altyn Tagh range during the development of east-striking Lapeiquan detachment fault (Chen et al., 2003). We suggest that the extensional event may have been induced by gravitational



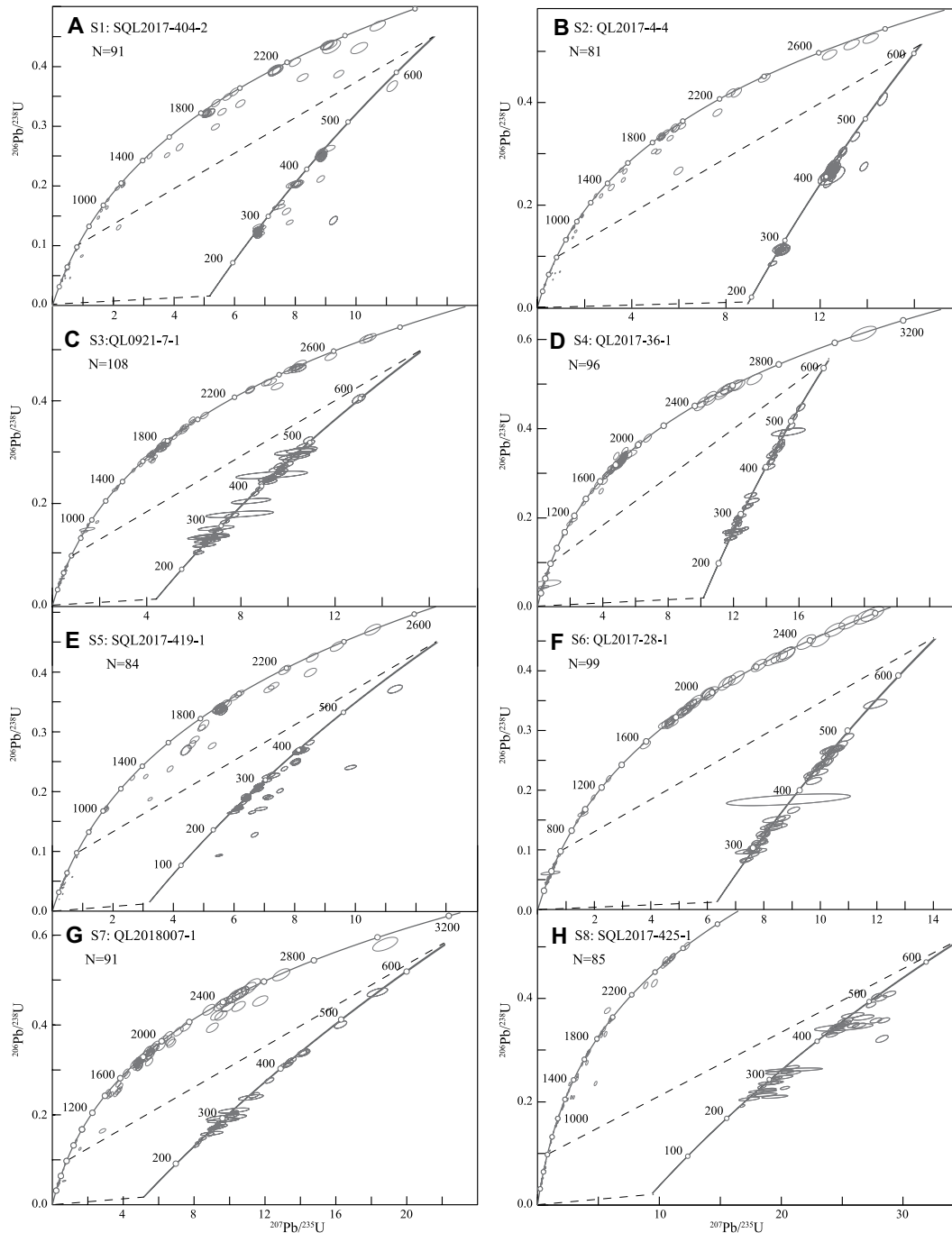


**Figure 15.** Laser ablation–multicollector–inductively coupled plasma–mass spectrometry U–Pb concordia diagrams for detrital zircon samples from Miocene (sample S1) and Lower Cretaceous (samples S2–S13) samples, Liyuanpu region, NW China.

collapse of a thickened continental lithosphere in northern Tibet.

### Stage 2B. Cretaceous Right-Slip Duplex Development

According to the regional structural relationship, the Liyuanpu fault postdates the Yumushan thrust and nappe system (Chen et al., 2019b). Its inferred right-slip faulting may have been coeval with extension along

the Hongshan fault (Fig. 12C). The Liyuanpu, Lanheba, Aohe and Qijiataizi faults that bound the Hongshan anticlinorium display a strike-slip duplex-like fault network, which is similar with the strike-slip duplex in northern Altyn Tagh (Cowgill et al., 2000). Right-slip faulting may have caused the distortion of the earlier folds, which may explain why the fold axis of the Aoheshan syncline changes its trend along the fold trace (Fig. 18). Regionally, the Hexi Corridor was proposed to have been bounded

by dextral motion of the North Qilian and Longshou Shan fault systems in Early Cretaceous (Vincent and Allen, 1999).

### Stage 3. Folding of Miocene Strata

The Cenozoic Indo-Asian collision affected vast regions of Asia from the Himalaya in the south to Lake Baikal in the north over a distance of more than 4000 km in the north-south direction (Molnar and Tapponnier, 1975; Tapponnier

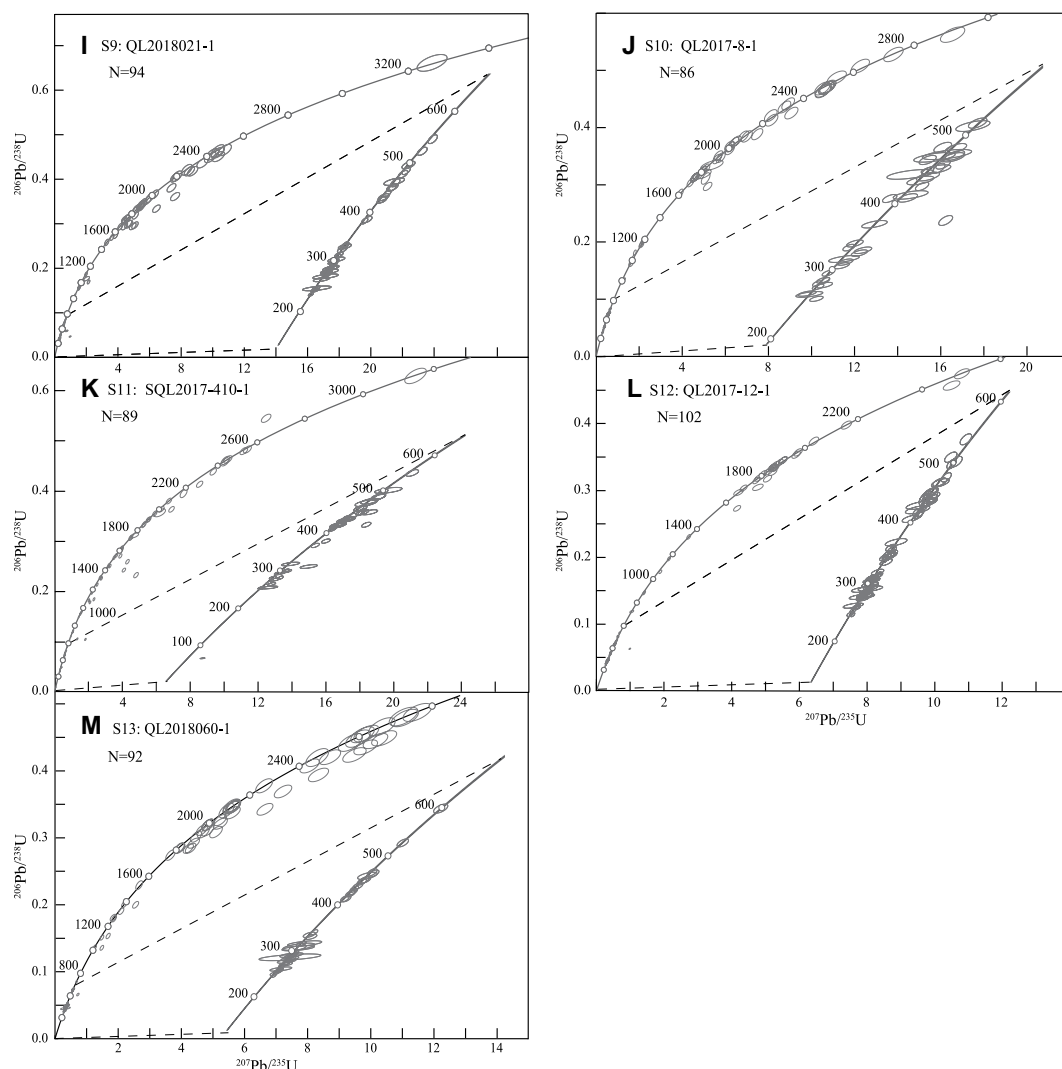


Figure 15. (Continued)

et al., 1990; Molnar, 1998; Yin and Harrison, 2000; Zhao et al., 2006; Clark et al., 2010; Yin, 2010; Najman et al., 2010; Wu et al., 2014; Hu et al., 2015b; Xu et al., 2016; Xiao et al., 2017; Wang et al., 2018; Colleps et al., 2020). During the initial of the Indo-Asian collision, the South Qilian and Nan Shan thrust belt started its activities along its southern margin against the Qaidam basin (65–50 Ma), and the left-slip Altyn Tagh fault was initiated at ca. 49 Ma (Yin et al., 2002, 2008a, 2008b). The basal sediments in the Qaidam basin (i.e., Lulehe Formation) are generally interpreted to be Eocene, which suggests thrust loading along its margins by the early Cenozoic (e.g., Chang et al., 2015; Ke et al., 2013; Yin et al., 2008a; Ji et al., 2017; Cheng et al., 2019b), although others have argued for an Oligocene-Miocene age for this formation (e.g., Wang et al., 2017). Apatite He cooling ages suggest that the southern margin of the Qaidam basin may have begun to rise

at ca. 35 Ma (Clark et al., 2010). The interior of the Qilian Shan-Nan Shan thrust belt experienced exhumation in the early Cenozoic (Li et al., 2020a), and detrital thermochronology from the northern foreland supports Eocene exhumation of parts of the Qilian Shan (An et al., 2020). The Qilian Shan-Nan Shan thrust belt expanded outward with the initiation of transpressional deformation associated with the Haiyuan fault at ca. 17–16 Ma, including initiation of the North Qilian thrust system (George et al., 2001; Wang et al., 2016; An et al., 2018; Lin et al., 2019; Li et al., 2019a, 2020a). The lack of the Upper Cretaceous and Paleogene strata in our study area indicates a period of tectonic quiescence from the Late Cretaceous to the middle Miocene (Li et al., 2019a). The formation of broad and gentle folds in the Miocene strata ( $N_1$ ) may be the result of the most recent northward expansion of the Qilian Shan-Nan Shan thrust belt.

### Source Areas of Cretaceous and Miocene Strata

Detrital zircon age spectra of the Lower Cretaceous strata (samples S2–S13 in Fig. 16 and Table 1) are dominated by two age clusters at 442–423 Ma and 297–266 Ma. The lack of detrital zircon ages of 0.8–0.9 Ga from the plutonic rocks of the interior part of the Qilian Shan-Nan Shan thrust belt (Zuza et al., 2018) led us to suggest that main source areas for the Cretaceous strata are from the region to the north, affected by the development of the Paleo-Asia orogenic system and the northern margin of the Qilian Shan-Nan Shan thrust belt. This suggestion is consistent with paleocurrent data derived in the Liyuanpu area, which implies Lower Cretaceous sediments were derived from both the Qilian Shan in the south and the Longshou Shan in the north (Vincent and Allen, 1999). The Alxa area to the north exposes Middle Ordovician–Early



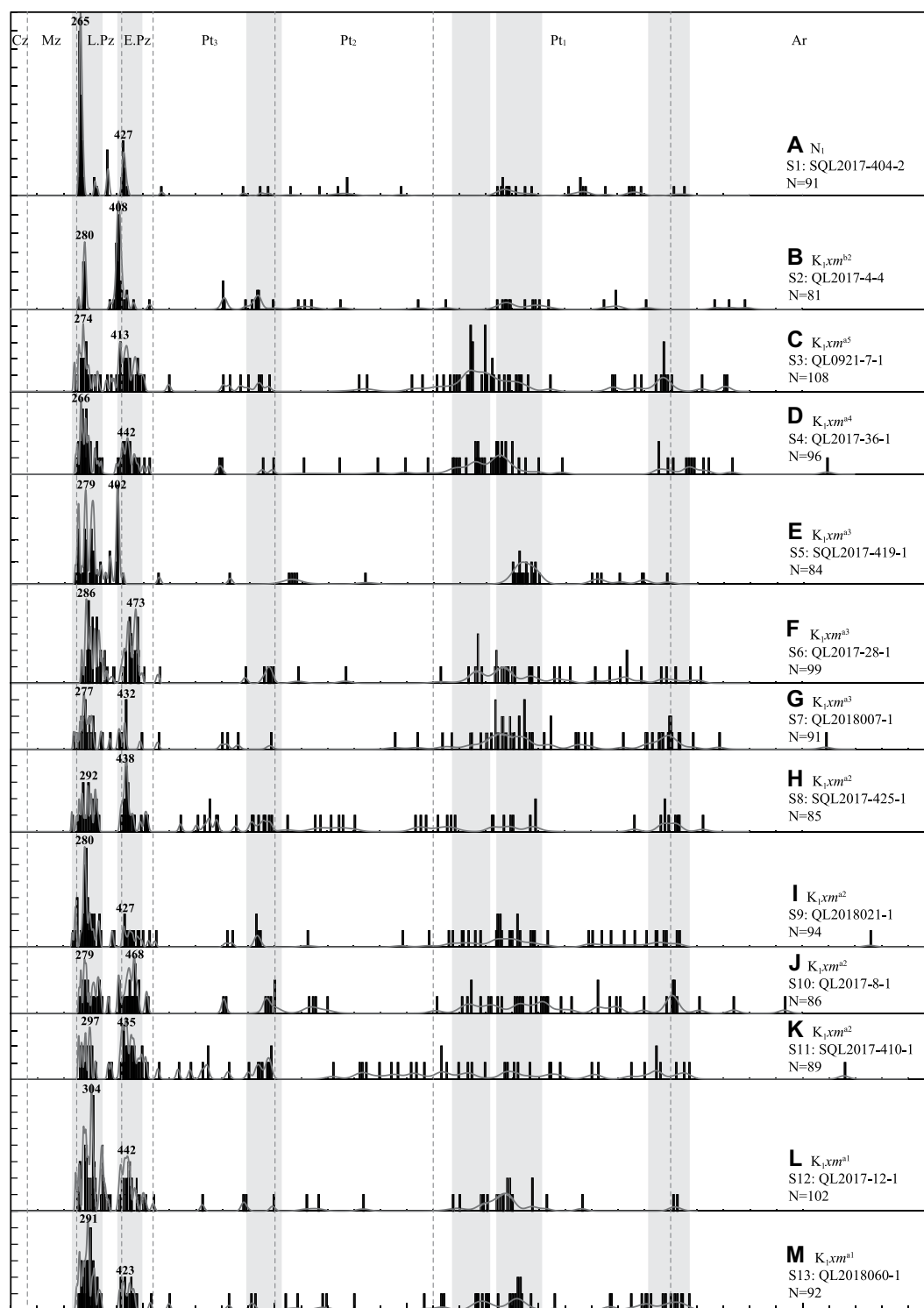


**Figure 16.** U-Pb age spectra of the detrital zircon samples from Miocene ( $N_1$ ) and Lower Cretaceous ( $K_1$ ) strata in the Liyuanpu region, NW China. Cz—Cenozoic; Mz—Mesozoic; L.Pz—Late Paleozoic; E.Pz—Early Paleozoic; Pt<sub>3</sub>—Neoproterozoic; Pt<sub>2</sub>—Mesoproterozoic; Pt<sub>1</sub>—Paleoproterozoic; Ar—Archean. Unit of age is Ma.

Devonian granitoids with ages of 461–441 Ma and 432–397 Ma (Fig. 2; Zhang and Gong, 2018; Wang et al., 2020). The Qilian Shan area exposes granitoids of ca. 500–420 Ma (Fig. 2; Xu et al., 1999; Gehrels et al., 2003a, 2003b, 2011; Wu et al., 2006, 2017; Cheng et al., 2019a; Liu et al., 2019). The Permian (297–266 Ma)

detrital zircon in the Cretaceous strata may have been derived from the late Paleozoic–early Mesozoic Badain Jaran magmatic arc in the Alxa area where Late Carboniferous–early Triassic (289–269 Ma) plutons are exposed (Fig. 2; Geng and Zhou, 2012; Chen et al., 2013; Zheng et al., 2014; Zhang et al., 2015; Shi et al., 2016; Liu

et al., 2017a). Following Cheng et al. (2019a), we suggest that the current topographic depression between the Qilian Shan and Longmen Shan was also a topographic depression in the Early Cretaceous. Some detrital zircons from the Lower Cretaceous strata yield Paleoproterozoic ages clustered at 2.58–2.47 Ga and 1.95–1.75 Ga

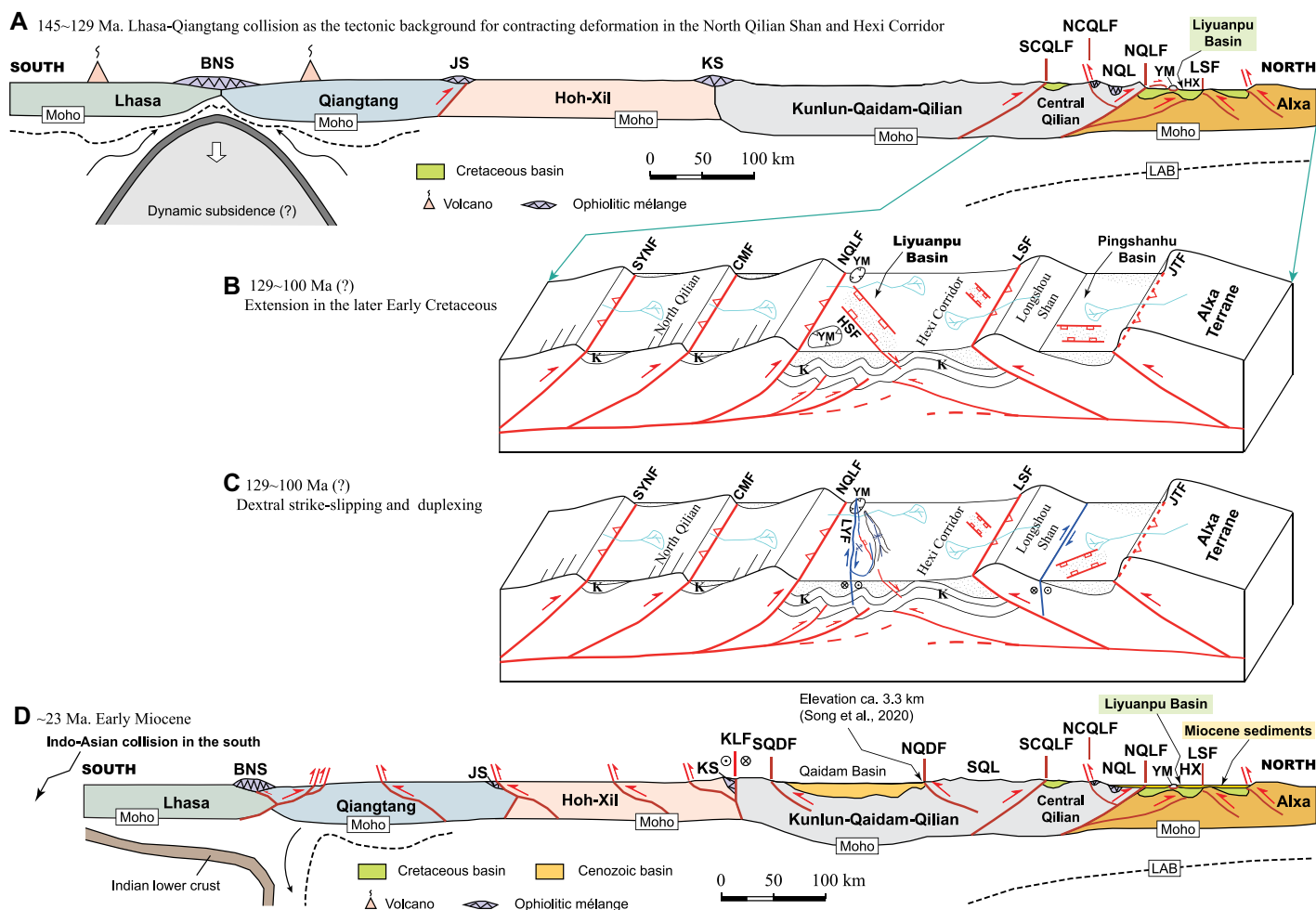


**Figure 17.** Tectonic evolution of the northern Qilian Shan and the Hexi Corridor, NW China since the Cretaceous. (A and D) are tectonic models for Early Cretaceous and early Miocene, respectively. Modified from Kapp and DeCelles (2019). (B and C) illustrate the extension and dextral strike-slip faulting in the late Early Cretaceous, respectively. NQL—North Qilian Shan; HX—Hexi Corridor; SQL—South Qilian Shan; YM—Yumu Shan; BNS—Bangong Co-Nujiang Suture; JS—Jinsha Suture; KS—Kunlun Suture; SCQLF—South Central Qilian fault; NCQLF—North Central Qilian fault; NQLF—North Qilian fault; LSF—Longshoushan fault; KLF—Kunlun fault; SQDF—South Qaidam fault; NQDF—North Qaidam fault; SYNF—South Yuniugou fault; CMF—Changma fault; JTF—Jinta fault; HSF—Hongshanshan fault; LYF—Liyuanpu fault; K—Cretaceous.

(Fig. 16). These ages are consistent with the ages of the Precambrian basement rocks in the Alxa area and North China north of our study area (Zhai and Santosh, 2011; Wu et al., 2005; Zhao et al., 2005, 2010, 2012; Jiang et al., 2010; Wan et al., 2014).

U-Pb detrital-zircon ages from the Miocene sediments (sample S1; Fig. 16A and Table 1) are dominated by a major ca. 265 Ma (Permian) age peak and minor ca. 427 Ma (Silurian) and ca. 367 Ma (Late Devonian) age peaks. These age peaks are similar to the ages of plutons (289–269 Ma) in the Alxa area (Fig. 2; Geng and Zhou, 2012), and the Beishan orogenic belt with granite plutons of 310 Ma to 230 Ma (Cheng et al., 2019a). Although Permo-Triassic plutons are present in the southern and central Qilian

Shan, they are separated from the northern Qilian Shan by a watershed in the range south of Yuniugou valley. The Alxa region north to the Hexi Corridor could have been a topographical height north of the Hexi Corridor before the rise of the northern Qilian Shan in the Miocene (Fig. 17D). In contrast, the northern Qaidam basin may have also been higher in the early Oligocene than the northern Qilian Shan (Song et al., 2020).

## CONCLUSIONS

In this study we address the problem of whether the northern margin region of the Tibetan plateau had experienced a compressional event in the Cretaceous. To answer this

question, we conducted detailed field mapping, stratigraphic description, U-Pb detrital zircon dating of Cretaceous strata, examination of growth-strata relationships, and construction and restoration of balanced cross sections. Our field mapping reveals multiple phases of deformation in the area since the Early Cretaceous, which was expressed by northwest-trending folding and northwest-striking thrusting that occurred at the early stage of the Early Cretaceous. The compressional event was followed immediately by extension and linked right-slip faulting in the later stage of the Early Cretaceous. The area underwent gentle northwest-trending folding since the late Miocene. We estimate the magnitude of the Early Cretaceous crustal shortening to be ~35%, which we interpret to have



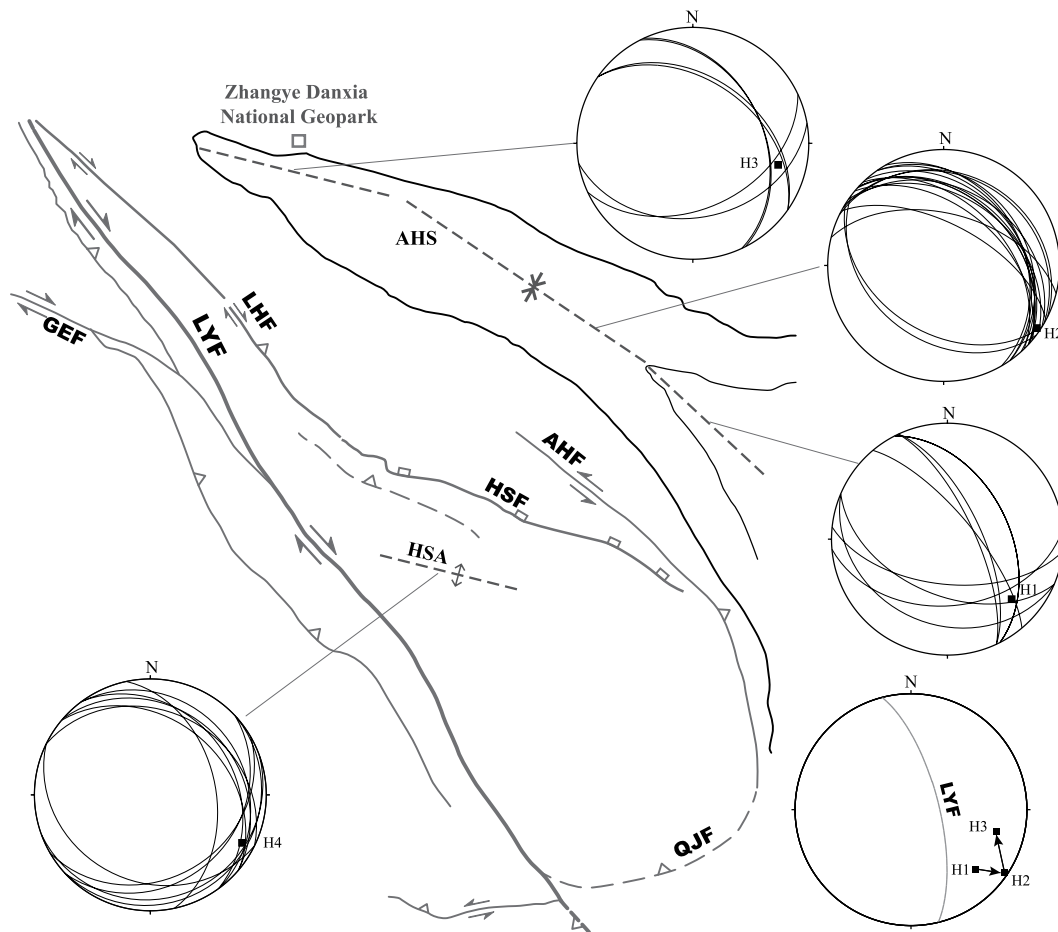


**Figure 18.** Stereographic projections for the Aoheshan syncline (AHS) and the Hongshan Anticlinorium (HSA), Liyuanpu region, NW China. H1, H2, and H3 are interpreted fold hinges for southeastern, central, and northwestern segments of the Aoheshan syncline, respectively, with changing of the plunges shown. H4 is the hinge for the Hongshan Anticlinorium. LYF—Liyuanpu fault; LHF—Lanheba fault; HSF—Hongshan fault; AHF—Aohe fault; QJF—Qijataizi fault; GEF—Gaoerwan fault.

resulted from a far-field response to the collision between the Lhasa and the Qiangtang terranes in the south. We suggest that the subsequent extension in the Early Cretaceous was induced by orogenic collapse. U-Pb dating of detrital zircons, from the Lower Cretaceous sedimentary clasts, suggests they were sourced from the north and the south, which implies the current foreland region of the Tibetan plateau was a topographic depression between two highland regions in the Early Cretaceous. Our work also shows that the Miocene strata in the foreland region of the northern Tibetan plateau was dominantly sourced from the north, which implies that the rise of the Qilian Shan did not impact the sediment dispersal in the current foreland region of the Tibetan plateau where this study was conducted.

#### ACKNOWLEDGMENTS

We would like to thank Zengzhen Wang, Feizhou Ma, Jian'en Han, Chengguang He, Jianjie Shi, Jianguo Li, Haohao Shao, Huixin Miao, Lele Han, and the Zhangye Danxia National Geopark for their help in the field work. Financial supports by the National Key Research and Development Program of China (the DREAM—Deep Resource Exploration

and Advanced Mining; no. 2018YFC0603701) and the China Geological Survey (nos. DD20160083 and DD20190011) are gratefully acknowledged. Critical comments and constructive suggestions of two anonymous reviewers led to significant improvement of the original manuscript.

#### REFERENCES CITED

- An, K., Lin, X., Wu, L., Cheng, X., Chen, H., Ding, W., Zhang, F., Gong, J., Yang, R., Zhu, K., Li, C., Zhang, Y., and Gao, S., 2018, Reorganization of sediment dispersal in the Jiuxi Basin at ~17 Ma and its implications for uplift of the NE Tibetan Plateau: *Palaeogeography, Palaeoclimatology, Palaeoecology*, v. 511, p. 558–576, <https://doi.org/10.1016/j.palaeo.2018.09.022>.
- An, K., Lin, X., Wu, L., Yang, R., Chen, H., Cheng, X., Xia, Q., Zhang, F., Ding, W., Gao, S., Li, C., and Zhang, Y., 2020, An immediate response to the Indian-Eurasian collision along the northeastern Tibetan Plateau: Evidence from apatite fission track analysis in the Kuantan Shan-Hei Shan: *Tectonophysics*, v. 774, p. 22827, <https://doi.org/10.1016/j.tecto.2019.22827>.
- Bally, A.W., Gordy, P.L., and Stewart, G.A., 1966, Structure, seismic data, and orogenic evolution of southern Canadian Rocky Mountains: *Bulletin of Canadian Petroleum Geology*, v. 14, no. 6, p. 337–381.
- Bureau of Geology of Gansu Province (BGGP, First Regional Geological Survey), 1971, *Geologic Map of Sunan Region*, scale 1:200,000: Beijing, China, Ministry of Geology of China.
- Bureau of Geology of Gansu Province (BGGP, First Regional Geological Survey), 1973, *Geologic Map of Zhangye Region*, scale 1:200,000: Beijing, China, Ministry of Geology of China.
- Bureau of Geology of Qinghai Province (BGQP, Regional Geological Survey), 1968, *Geologic Map of Yendiutai Region*, scale 1:200,000: Beijing, China, Ministry of Geology of China.
- Cao, Y., Sun, Z.M., Li, H.B., Pei, J.L., Liu, D.L., Zhang, L., Ye, X.Z., Zheng, Y., He, X.L., Ge, C.L., and Jiang, W., 2019, New paleomagnetic results from Middle Jurassic limestones of the Qiangtang Terrane, Tibet: Constraints on the evolution of the Bangong Nui-Jiang Ocean: *Tectonics*, v. 38, p. 215–232, <https://doi.org/10.1029/2017TC004842>.
- Chang, H., Li, L., Qiang, X., Garzione, C.N., Pullen, A., and An, Z., 2015, Magnetostratigraphy of Cenozoic deposits in the western Qaidam Basin and its implication for the surface uplift of the northeastern margin of the Tibetan Plateau: *Earth and Planetary Science Letters*, v. 430, p. 271–283, <https://doi.org/10.1016/j.epsl.2015.08.029>.
- Chen, S., Wang, H., Wei, J., Lv, Z., Gan, H., and Jin, S., 2014a, Sedimentation of the Lower Cretaceous Xiagou Formation and its response to regional tectonics in the Qingxi Sag, Jiuquan Basin, NW China: *Cretaceous Research*, v. 47, p. 72–86, <https://doi.org/10.1016/j.cretres.2013.11.006>.
- Chen, W., Zhou, W.P., Chen, K.X., Liu, M.W., Wang, T., Fang, M., He, H.Y., and Zhang, B., 2013, Subduction-related early Permian granodiorite in Jinchangshan of Alashan, Inner Mongolia: Evidences from zircon U-Pb geochronology and geochemistry [in Chinese with English abstract]: *Journal of Mineralogy and Petrology*, v. 33, p. 53–60.
- Chen, X.H., Yin, A., Gehrels, G.E., Cowgill, E.S., Grove, M., Harrison, T.M., and Wang, X.F., 2003, Two phases of Mesozoic north-south extension in the eastern Altyn Tagh range, northern Tibetan Plateau: *Tectonics*, v. 22, no. 5, <https://doi.org/10.1029/2001TC001336>.

- Chen, X.H., Dang, Y.Q., Yin, A., Wang, L.Q., Jiang, W.M., Jiang, R.B., Zhou, S.P., Liu, M.D., Ye, B.Y., Zhang, M., Ma, L.X., and Li, L., 2010, Basin-Mountain Coupling and Tectonic Evolution of the Qaidam Basin and its Adjacent Orogenic Belts [in Chinese]: Beijing, China, Geological Publishing House, 365 p.
- Chen, X.H., Gehrels, G.E., Yin, A., Li, L., and Jiang, R.B., 2012, Paleozoic and Mesozoic basement magmatism of Eastern Qaidam Basin, northern Qinghai-Tibet Plateau: LA-ICP-MS Zircon U-Pb geochronology and its geological significance: *Acta Geologica Sinica*, v. 86, p. 350–369, <https://doi.org/10.1111/j.1755-6724.2012.00665.x>.
- Chen, X.H., Gehrels, G., Yin, A., Zhou, Q., and Huang, P.H., 2015, Geochemical and Nd-Sr-Pb-O isotopic constraints on Permo-Triassic magmatism in eastern Qaidam Basin, northern Qinghai-Tibetan plateau: Implications for the evolution of the Paleo-Tethys: *Journal of Asian Earth Sciences*, v. 114, p. 674–692, <https://doi.org/10.1016/j.jseas.2014.11.013>.
- Chen, X.H., Shao, Z.G., Xiong, X.S., Gao, R., Liu, X.J., Wang, C.F., Li, B., Wang, Z.Z., and Zhang, Y.P., 2019a, Fault system, deep structure and tectonic evolution of the Qilian Orogenic Belt, Northwest China [in Chinese with English abstract]: *Geology in China*, v. 46, p. 995–1020.
- Chen, X.H., Shao, Z.G., Xiong, X.S., Gao, R., Xu, S.L., Zhang, Y.P., Li, B., and Wang, Y., 2019b, Early Cretaceous overthrusting of Yumushan Mountain and hydrocarbon prospecting in northern margin of the Qilian Orogenic Belt [in Chinese with English abstract]: *Acta Geoscientia Sinica*, v. 40, p. 377–392.
- Chen, Y., Song, S., Niu, Y., and Wei, C., 2014b, Melting of continental crust during subduction initiation: A case study from the Chaidanuo peraluminous granite in the North Qilian suture zone: *Geochimica et Cosmochimica Acta*, v. 132, p. 311–336, <https://doi.org/10.1016/j.gca.2014.02.011>.
- Chen, Y.F., Ding, L., Li, Z.Y., Laskowski, A.K., Li, J.X., Baral, U., Qasim, M., and Yue, Y.H., 2020, Provenance analysis of Cretaceous peripheral foreland basin in central Tibet: Implications to precise timing on the initial Lhasa-Qiangtang collision: *Tectonophysics*, v. 775, no. 228311, <https://doi.org/10.1016/j.tecto.2019.228311>.
- Cheng, F., Garzone, C., Jolivet, M., Wang, W.T., Dong, J.B., Richter, F., and Guo, Z.J., 2019a, Provenance analysis of the Yumen Basin and northern Qilian Shan: Implications for the pre-collisional paleogeography in the NE Tibetan plateau and eastern termination of Altyn Tagh fault: *Gondwana Research*, v. 65, p. 156–171, <https://doi.org/10.1016/j.gr.2018.08.009>.
- Cheng, F., Jolivet, M., Guo, Z., Lu, H., Zhang, B., Li, X., Zhang, D., Zhang, C., Zhang, H., Wang, L., Wang, Z., and Zhang, Q., 2019b, Jurassic–Early Cenozoic tectonic inversion in the Qilian Shan and Qaidam Basin, North Tibet: New insight from seismic reflection, isopach mapping, and drill core data: *Journal of Geophysical Research. Solid Earth*, v. 124, p. 12077–12098, <https://doi.org/10.1029/2019JB018086>.
- China Geological Survey, 2004, Geological Map of the People's Republic of China (1:2,500,000) [in Chinese]: Beijing, China, SinoMaps Press.
- Clark, M.K., Farley, K.A., Zheng, D., Wang, Z., and Duvall, A.R., 2010, Early Cenozoic faulting of the northern Tibetan Plateau margin from apatite (U-Th)/He ages: *Earth and Planetary Science Letters*, v. 296, p. 78–88, <https://doi.org/10.1016/j.epsl.2010.04.051>.
- Colleges, C.L., McKenzie, N.R., Horton, B.K., Webb, A.A.G., Ng, Y.W., and Singh, B.P., 2020, Sediment provenance of pre- and post-collisional Cretaceous–Paleogene strata from the frontal Himalaya of northwest India: *Earth and Planetary Science Letters*, v. 534, no. 116079, <https://doi.org/10.1016/j.epsl.2020.116079>.
- Cowgill, E., Yin, A., Feng, W.X., and Qing, Z., 2000, Is the North Altyn fault part of a strike-slip duplex along the Altyn Tagh fault system?: *Geology*, v. 28, no. 3, p. 255–258, [https://doi.org/10.1130/0091-7613\(2000\)28<255:ITNAFF>2.0.CO;2](https://doi.org/10.1130/0091-7613(2000)28<255:ITNAFF>2.0.CO;2).
- Dahlstrom, C.D.A., 1969, Balanced cross section: *Canadian Journal of Earth Sciences*, v. 6, p. 743–757, <https://doi.org/10.1139/e69-069>.
- Duan, J., Li, C., Qian, Z., and Jiao, J.G., 2015, Geochronological and geochemical constraints on the petrogenesis and tectonic significance of Paleozoic dolerite dykes in the southern margin of Alxa Block, North China Craton: *Journal of Asian Earth Sciences*, v. 111, p. 244–253, <https://doi.org/10.1016/j.jseas.2015.07.012>.
- Dupont-Nivet, G., Horton, B.K., Butler, R.F., Wang, J., Zhou, J., and Waanders, G.L., 2004, Paleogene clockwise tectonic rotation of the Xining-Lanzhou region, northeastern Tibetan Plateau: *Journal of Geophysical Research. Solid Earth*, v. 109, no. B4, <https://doi.org/10.1029/2003JB002913>.
- England, P., and Houseman, G., 1986, Finite strain calculations of continental deformation: 2. Comparison with the India-Asia collision zone: *Journal of Geophysical Research*, v. 91, no. B3, p. 3664–3676, <https://doi.org/10.1029/JB091iB03p03664>.
- Frost, G.M., Coe, R.S., Meng, Z., Peng, Z., Chen, Y., Courtillot, V., Peltzer, G., Tapponnier, P., and Avouac, J.-P., 1995, Preliminary Early Cretaceous paleomagnetic results from the Gansu Corridor, China: *Earth and Planetary Science Letters*, v. 129, p. 217–232, [https://doi.org/10.1016/0012-821X\(94\)00244-5](https://doi.org/10.1016/0012-821X(94)00244-5).
- Fu, C., Yan, Z., Aitchison, J.C., Xiao, W., Buckman, S., Wang, B., Li, W., Li, Y., and Ren, H., 2020, Multiple subduction processes of the Proto-Tethyan Ocean: Implication from Cambrian intrusions along the North Qilian suture zone: *Gondwana Research*, v. 87, p. 207–223, <https://doi.org/10.1016/j.gr.2020.06.007>.
- Gao, R., Wang, H.Y., Yin, A., Dong, S.W., Kuang, Z.Y., Zuza, A.V., Li, W.H., and Xiong, X.S., 2013, Tectonic development of the northeastern Tibetan Plateau as constrained by high-resolution deep seismic-reflection data: *Lithosphere*, v. 5, p. 555–574, <https://doi.org/10.1130/L293.1>.
- Gehrels, G.E., Yin, A., and Wang, X.F., 2003a, Detrital-zircon geochronology of the northeastern Tibetan Plateau: *Geological Society of America Bulletin*, v. 115, p. 881–896, [https://doi.org/10.1130/0016-7606\(2003\)115<0881:DGOTNT>2.0.CO;2](https://doi.org/10.1130/0016-7606(2003)115<0881:DGOTNT>2.0.CO;2).
- Gehrels, G.E., Yin, A., and Wang, X.F., 2003b, Magmatic history of the northeastern Tibetan Plateau: *Journal of Geophysical Research. Solid Earth*, v. 108, no. B9, <https://doi.org/10.1029/2002JB001876>.
- Gehrels, G.E., Kapp, P., DeCelles, P., Pullen, A., Blakey, R., Weislogel, A., Ding, L., Guynn, J., Martin, A., McQuarrie, N., and Yin, A., 2011, Detrital zircon geochronology of pre-Tertiary strata in the Tibetan-Himalayan orogen [T.C.]: *Tectonics*, v. 30, no. 5, <https://doi.org/10.1029/2011TC002868>.
- Geng, Y.S., and Zhou, X.W., 2012, Early Permian magmatic events in the Alxa metamorphic basement: Evidence from geochronology [in Chinese with English abstract]: *Yanshi Xuebao*, v. 28, p. 2667–2685.
- George, A.D., Marshall, S.J., Wyrwoll, K.H., Jie, C., and Yanchou, L., 2001, Miocene cooling in the northern Qilian Shan, northeastern margin of the Tibetan Plateau, revealed by apatite fission-track and vitrinite-reflection analysis: *Geology*, v. 29, p. 939–942, [https://doi.org/10.1130/0091-7613\(2001\)029<0939:MCITNQ>2.0.CO;2](https://doi.org/10.1130/0091-7613(2001)029<0939:MCITNQ>2.0.CO;2).
- Gong, J.H., Zhang, J.X., Yu, S.Y., Li, H.K., and Hou, K.J., 2012, ~2.5 Ga TTG gneiss and its geological implications in the western Alxa block, North China Craton: *Chinese Science Bulletin*, v. 57, p. 4064–4076, <https://doi.org/10.1007/s11434-012-5315-8>.
- Heubeck, C., 2001, Assembly of Central Asia during the middle and late Paleozoic, in Hendrix, M.S., and Davis, G.A., eds., *Paleozoic and Mesozoic Tectonic Evolution of Central Asia: From Continental Assembly to Intracontinental Deformation*: Geological Society of America Memoir, v. 194, p. 1–22, <https://doi.org/10.1130/0-8137-1194-0.1>.
- Hu, N.G., Xu, A.D., and Yang, J.X., 2005, Characteristics and tectonic environment of Zhigoumen pluton in Longshouan area [in Chinese with English abstract]: *Diqu Kexue Yu Huanjing Xuebao*, v. 27, p. 5–11.
- Hu, X.M., Garzanti, E., Moore, T., and Raffi, I., 2015b, Direct stratigraphic dating of India-Asia collision onset at the Selandian (middle Paleocene, 59 ± 1 Ma): *Geology*, v. 43, p. 859–862, <https://doi.org/10.1130/G36872.1>.
- Hu, Z.C., Zhang, W., Liu, Y.S., Gao, S., Li, M., Zong, K.Q., Chen, H.L., and Hu, S.H., 2015a, “Wave” signal-smoothing and mercury-removing device for laser ablation quadrupole and multiple collector ICPMS analysis: Application to lead isotope analysis [in Chinese with English abstract]: *Analytical Chemistry*, v. 87, p. 1152–1157, <https://doi.org/10.1021/ac503749k>.
- Hui, J., Cheng, H., Zhang, J., Zhang, K., Qu, J., and Zhang, B., 2020, Early Cretaceous continent basalts in the Alxa Block, NW China: Geochronology, geochemistry, and tectonic implications: *International Geology Review*, <https://doi.org/10.1080/00206814.2020.1734974>.
- Ji, J., Zhang, K., Clift, P.D., Zhuang, G., Song, B., Ke, X., and Xu, Y., 2017, High-resolution magnetostratigraphic study of the Paleogene-Neogene strata in the Northern Qaidam Basin: Implications for the growth of the Northeastern Tibetan Plateau: *Gondwana Research*, v. 46, p. 141–155, <https://doi.org/10.1016/j.gr.2017.02.015>.
- Jiang, N., Guo, J.H., Zhai, M.G., and Zhang, S.Q., 2010, ~2.7 Ga crust growth in the North China craton: Precambrian Research, v. 179, p. 37–49, <https://doi.org/10.1016/j.precamres.2010.02.010>.
- Jolivet, M., Brunel, M., Seward, D., Xu, Z., Yang, J., Roger, F., Tapponnier, P., Malavieille, J., Arnaud, N., and Wu, C., 2001, Mesozoic and Cenozoic tectonics of the northern edge of the Tibetan plateau: Fission-track constraints: *Tectonophysics*, v. 343, p. 111–134, [https://doi.org/10.1016/S0040-1951\(01\)00196-2](https://doi.org/10.1016/S0040-1951(01)00196-2).
- Kapp, P., and DeCelles, P.G., 2019, Mesozoic–Cenozoic geological evolution of the Himalayan-Tibetan Orogen and working tectonic hypotheses: *American Journal of Science*, v. 319, p. 159–254, <https://doi.org/10.2475/03.2019.01>.
- Kapp, P., Murphy, M.A., Yin, A., Harrison, T.M., Ding, L., and Guo, J.H., 2003, Mesozoic and Cenozoic tectonic evolution of the Shiquanhe area of western Tibet: *Tectonics*, v. 22, no. 4, <https://doi.org/10.1029/2001TC001332>.
- Kapp, P., DeCelles, P.G., Gehrels, G.E., Heizler, M., and Ding, L., 2007, Geological records of the Lhasa-Qiangtang and Indo-Asian collisions in the Nima area of central Tibet: *Geological Society of America Bulletin*, v. 119, p. 917–932, <https://doi.org/10.1130/B26033.1>.
- Kazmin, V.G., 1991, Collision and rifting in the Tethys Ocean: Geodynamic implications: *Tectonophysics*, v. 196, p. 371–384, [https://doi.org/10.1016/0040-1951\(91\)90331-L](https://doi.org/10.1016/0040-1951(91)90331-L).
- Ke, X., Ji, J., Zhang, K., Kou, X., Song, B., and Wang, C., 2013, Magnetostratigraphy and Anisotropy of Magnetic Susceptibility of the Lulehe Formation in the Northeastern Qaidam Basin: *Acta Geologica Sinica*, v. 87, no. 2, p. 576–587, <https://doi.org/10.1111/1755-6724.12069>.
- Lai, W., Hu, X.M., Garzanti, E., Xu, Y.W., Ma, A.L., and Li, W., 2019, Early Cretaceous sedimentary evolution of the northern Lhasa terrane and the timing of initial Lhasa-Qiangtang collision: *Gondwana Research*, v. 73, p. 136–152, <https://doi.org/10.1016/j.gr.2019.03.016>.
- Li, B., Chen, X., Zuza, A.V., Hu, D., Ding, W., Huang, P., and Xu, S., 2019a, Cenozoic cooling history of the North Qilian Shan, northern Tibetan Plateau, and the initiation of the Haiyuan fault: Constraints from apatite- and zircon-fission track thermochronology: *Tectonophysics*, v. 751, p. 109–124, <https://doi.org/10.1016/j.tecto.2018.12.005>.
- Li, B., Zuza, A.V., Chen, X.H., Hu, D.G., Shao, Z.G., Qi, B.-S., Wang, Z.Z., Levy, D.A., and Xiong, X.S., 2020a, Cenozoic multi-phase deformation in the Qilian Shan and out-of-sequence development of the northern Tibetan Plateau: *Tectonophysics*, v. 782–783, no. 228423, <https://doi.org/10.1016/j.tecto.2020.228423>.
- Li, B., Zuza, A.V., Chen, X.H., Wang, Z.Z., Shao, Z.G., Levy, D.A., Wu, C., Xu, S.L., and Sun, Y.J., 2021, Pre-Cenozoic evolution of the northern Qilian Orogen from zircon geochronology: Framework for early growth of the northern Tibetan Plateau: *Palaeogeography, Palaeoclimatology, Palaeoecology*, v. 562, no. 110091, <https://doi.org/10.1016/j.palaeo.2020.110091>.
- Li, F.Q., 2003, New evidence for the presence of the NS-trending extensional structures in northwestern China: An example from the Early Cretaceous half graben fault depressions in Jiuguang, Gansu [in Chinese with English abstract]: *Chenji Yu Tetisi Dizhi*, v. 23, no. 2, p. 35–42.



- Li, G.W., Sandiford, M., Fang, A.-M., Kohn, B., Sandiford, D., Fu, B.-H., Zhang, T.L., Cao, Y.Y., and Chen, F., 2019b, Multi-stage exhumation history of the West Kunlun orogen and the amalgamation of the Tibetan Plateau: Earth and Planetary Science Letters, v. 528, no. 115833, <https://doi.org/10.1016/j.epsl.2019.115833>.
- Li, H.K., Geng, J.Z., Hao, S., Zhang, Y.Q., and Li, H.M., 2009, Study on the determination of U-Pb isotopic age of zircon by laser ablation multi-collector inductively LA-MC-ICPMS [in Chinese]: Acta Mineralogica Sinica, v. 29, no. S1, p. 600–601.
- Li, S., Guilmette, C., Yin, C.Q., Ding, L., Zhang, J., Wang, H.Q., and Baral, U., 2019c, Timing and mechanism of Bangong-Nujiang ophiolite emplacement in the Gerze area of central Tibet: Gondwana Research, v. 71, p. 179–193, <https://doi.org/10.1016/j.gr.2019.01.019>.
- Li, S., Yin, C.Q., Ding, L., Guilmette, C., Zhang, J., Yue, Y.H., and Baral, U., 2020b, Provenance of Lower Cretaceous sedimentary rocks in the northern margin of the Lhasa terrane, Tibet: Implications for the timing of the Lhasa-Qiangtang collision: Journal of Asian Earth Sciences, v. 190, p. 104162, <https://doi.org/10.1016/j.jseas.2019.104162>.
- Liao, H., Hu, D.G., Zhang, X.J., Yu, W.L., and Guo, T., 2014, Zircon U-Pb age for granite of the Ordovician formation and its tectonic significance in the southern Qilianshan [in Chinese with English abstract]: Journal of Geology, v. 20, no. 3, p. 293–298.
- Licht, A., van Cappelle, M., Abels, H.A., Ladant, J.B., Trabucchi-Alexandre, J., France-Lanord, C., Donnadieu, Y., Vandenbergh, J., Rigaudier, T., Lecuyer, C., Terry, D., Jr., Adriaens, R., Boura, A., Guo, Z., Soe, A.N., Quade, J., Dupont-Nivet, G., and Jaeger, J.J., 2014, Asian monsoons in a late Eocene greenhouse world: Nature, v. 513, no. 7519, p. 501–506, <https://doi.org/10.1038/nature13704>.
- Lin, X., Tian, Y.T., Donelick, R.A., Liu, Z.J., Cleber, S.J., Li, C.A., Wu, Q.Y., and Li, Z.N., 2019, Mesozoic and Cenozoic tectonics of the northeastern edge of the Tibetan plateau: Evidence from modern river detrital apatite fission-track age constraints: Journal of Asian Earth Sciences, v. 170, p. 84–95, <https://doi.org/10.1016/j.jseas.2018.10.028>.
- Liu, C.F., Wu, C., Song, Z.J., Liu, W.C., and Zhang, H.Y., 2019, Petrogenesis and tectonic significance of Early Paleozoic magmatism in the northern margin of the Qilian block, northeastern Tibetan Plateau: Lithosphere, v. 11, p. 365–385, <https://doi.org/10.1130/L1047.1>.
- Liu, D., Yan, M., Fang, X., Li, H., Song, C., and Dai, S., 2011, Magnetostratigraphy of sediments from the Yumu Shan, Hexi Corridor and its implications regarding the Late Cenozoic uplift of the NE Tibetan Plateau: Quaternary International, v. 236, p. 13–20, <https://doi.org/10.1016/j.quaint.2010.12.007>.
- Liu, Q., Zhao, G.C., Sun, M., Han, Y.G., Eizenhöfer, P.R., Hou, W.Z., Zhang, X.R., Zhu, Y.L., Wang, B., Liu, D.X., and Xu, B., 2016, Early Paleozoic subduction processes of the Paleo-Asian Ocean: Insights from geochronology and geochemistry of Paleozoic plutons in the Alxa Terrane: Lithos, v. 262, p. 546–560, <https://doi.org/10.1016/j.lithos.2016.07.041>.
- Liu, Q., Zhao, G.C., Han, Y.G., Eizenhöfer, P.R., Zhu, Y.L., Hou, W.Z., and Zhang, X.R., 2017a, Timing of the final closure of the Paleo-Asian Ocean in the Alxa Terrane: Constraints from geochronology and geochemistry of Late Carboniferous to Permian gabbros and diorites: Lithos, v. 274–275, p. 19–30, <https://doi.org/10.1016/j.lithos.2016.12.029>.
- Liu, Q., Zhao, G., Han, Y., Eizenhöfer, P.R., Zhu, Y., Hou, W., Zhang, X., and Wang, B., 2017b, Geochronology and geochemistry of Permian to Early Triassic granitoids in the Alxa Terrane: Constraints on the final closure of the Paleo-Asian Ocean: Lithosphere, v. 9, no. 4, p. 665–680, <https://doi.org/10.1130/L646.1>.
- Liu, Y.S., Hu, Z.C., Gao, S., Günther, D., Xu, J., Gao, C.G., and Chen, H.H., 2008, In situ analysis of major and trace elements of anhydrous minerals by LA-ICP-MS without applying an internal standard: Chemical Geology, v. 257, p. 34–43, <https://doi.org/10.1016/j.chemgeo.2008.08.004>.
- Ludwig, K.R., 2003, User's Manual for Isoplot 3.00: A Geochronological Toolkit for Microsoft Excel: Berkeley Geochronological Center Special Publication, no. 4, p. 25–32.
- Ma, Y.M., Yang, T.S., Bian, W.W., Jin, J.J., Wang, Q., Zhang, S.H., Wu, H.C., Li, H.Y., and Cao, L.W., 2018, A stable southern margin of Asia during the Cretaceous: Paleomagnetic constraints on the Lhasa-Qiangtang collision and the maximum width of the Neo-Tethys: Tectonics, v. 37, p. 3853–3876, <https://doi.org/10.1029/2018TC005143>.
- Metcalfe, I., 2013, Gondwana dispersion and Asian accretion: Tectonic and palaeogeographic evolution of eastern Tethys: Journal of Asian Earth Sciences, v. 66, p. 1–33, <https://doi.org/10.1016/j.jseas.2012.12.020>.
- Molnar, P., 1998, A review of geophysical constraints on the deep structure of the Tibetan Plateau, the Himalaya and the Karakoram, and their tectonic implications: Philosophical Transactions-Royal Society, Mathematical, Physical, and Engineering Sciences, v. 326, p. 33–88.
- Molnar, P., and Tappin, P., 1975, Cenozoic tectonics of Asia: Effects of a continental collision: Science, v. 189, no. 4201, p. 419–426, <https://doi.org/10.1126/science.189.4201.419>.
- Murphy, M.A., Yin, A., Harrison, T.M., Dürr, S.B., Chen, Z., Ryerson, F.J., Kidd, W.S.F., Wang, X., and Zhou, X., 1997, Did the Indo-Asian collision alone create the Tibetan plateau?: Geology, v. 25, p. 719–722, [https://doi.org/10.1130/0091-7613\(1997\)025<0719:DTIAC>2.3.CO;2](https://doi.org/10.1130/0091-7613(1997)025<0719:DTIAC>2.3.CO;2).
- Najman, Y., Appel, E., Boudagher-Fadel, M., Bown, P., Carter, A., Garzanti, E., Godin, L., Han, J., Liebke, U., Oliver, G., Parrish, R., and Vezzoli, G., 2010, Timing of India-Asia collision: Geological, biostratigraphic, and palaeomagnetic constraints: Journal of Geophysical Research, Solid Earth, v. 115, no. B12, <https://doi.org/10.1029/2010JB007673>.
- Pan, G.T., and Xiao, Q.H., 2015, Tectonic Map of China (1:2,500,000) [in Chinese]: Beijing, China, Geological Publishing House.
- Qi, B.S., Hu, D.G., Yang, X.X., Zhang, Y.L., Tan, C.X., Zhang, P., and Feng, C.J., 2016, Apatite fission track evidence for the Cretaceous–Cenozoic cooling history of the Qilian Shan (NW China) and for stepwise northeastward growth of the northeastern Tibetan Plateau since early Eocene: Journal of Asian Earth Sciences, v. 124, p. 28–41, <https://doi.org/10.1016/j.jseas.2016.04.009>.
- Qin, H.P., 2012, Petrology of Early Paleozoic granites and their relation to tectonic evolution of orogen in the North Qilian Orogenic Belt [Ph.D. thesis] [in Chinese with English abstract]: Beijing, China, Chinese Academy of Geological Sciences.
- Raymo, M.E., and Ruddiman, W.F., 1992, Tectonic forcing of late Cenozoic climate: Nature, v. 359, p. 117–122, <https://doi.org/10.1038/359117a0>.
- Ryan, W.B.F., Carbotte, S.M., Coplan, J.O., O'Hara, S., Melkonian, A., Arko, R., Weissel, R.A., Ferrini, V., Goodwillie, A., Nitsche, F., Bonczkowski, J., and Zernsky, R., 2009, Global Multi-Resolution Topography synthesis: Geochemistry, Geophysics, Geosystems, v. 10, no. 3, <https://doi.org/10.1029/2008GC003232>.
- Şengör, A.M.C., and Natal'in, B.A., 1996a, Paleotectonics of Asia: Fragments of a synthesis, in Yin, A., and Harrison, T.M., eds., The Tectonics of Asia: New York, USA, Cambridge University Press, p. 486–640.
- Şengör, A.M., and Natal'in, B.A., 1996b, Turkic-type orogeny and its role in the making of the continental crust: Annual Review of Earth and Planetary Sciences, v. 24, p. 263–337, <https://doi.org/10.1146/annurev.earth.24.1.263>.
- Shao, H.H., Chen, X.H., Zhang, D., Shao, Z.G., Li, B., Wang, Z.Z., Zhang, Y.P., Xu, S.L., Shi, J.J., and Miao, H.X., 2019, The Early Cretaceous tectonic deformation stages and detrital zircon U-Pb ages of Pingshanhu Basin in Hexi Corridor [in Chinese with English abstract]: Geology in China, v. 46, p. 1079–1093.
- Shi, G.Z., Song, G.Z., Wang, H., Huang, C.Y., Zhang, L.D., and Tang, J.R., 2016, Late Paleozoic tectonics of the Solonker zone in the Wuliji area, Inner Mongolia, China: Insights from stratigraphic sequence, chronology, and sandstone geochemistry: Journal of Asian Earth Sciences, v. 127, p. 100–118, <https://doi.org/10.1016/j.jseas.2016.06.022>.
- Shi, J.P., Huo, T.F., Lai, Q., Peng, X.H., Du, S.Y., and Yang, D.B., 2015, Petrogenesis of Early Silurian Gangchadasi granites in the eastern segment of the northern South Qilian Block: Constraints from LA-ICP-MS zircon U-Pb geochronology and geochemistry [in Chinese with English abstract]: Acta Geoscientia Sinica, v. 36, no. 6, p. 781–789.
- Song, B.W., Spicer, R.A., Zhang, K.X., Ji, J.L., Farnsworth, A., Hughes, A.C., Yang, Y.B., Han, F., Xu, Y.D., Spicer, T., Shen, T.Y., Lunt, D.J., and Shi, G.L., 2020, Qaidam Basin leaf fossils show northeastern Tibet was high, wet and cool in the early Oligocene: Earth and Planetary Science Letters, v. 537, no. 116175, <https://doi.org/10.1016/j.epsl.2020.116175>.
- Song, S.G., Zhang, L.F., Niu, Y.L., Su, L., Song, B., and Liu, D.Y., 2006, Evolution from oceanic subduction to continental collision: A case study from the Northern Tibetan Plateau based on geochemical and geochronological data: Journal of Petrology, v. 47, p. 435–455, <https://doi.org/10.1093/petrology/egi080>.
- Song, S.G., Zhang, L.F., Niu, Y.L., Wei, C.J., Liou, J.G., and Shu, G.M., 2007, Eclogite and carpholite-bearing metasedimentary rocks in the North Qilian suture zone, NW China: Implications for Early Paleozoic cold oceanic subduction and water transport into mantle: Journal of Metamorphic Geology, v. 25, p. 547–563, <https://doi.org/10.1111/j.1525-1314.2007.00713.x>.
- Song, S.G., Niu, Y.L., Su, L., and Xia, X.H., 2013, Tectonics of the North Qilian orogen, NW China: Gondwana Research, v. 23, p. 1378–1401, <https://doi.org/10.1016/j.gr.2012.02.004>.
- Song, S.G., Niu, Y.L., Su, L., Zhang, C., and Zhang, L.F., 2014, Continental orogenesis from ocean subduction, continent collision/subduction, to orogen collapse, and orogen recycling: The example of the North Qaidam UHPM belt, NW China: Earth-Science Reviews, v. 129, p. 59–84, <https://doi.org/10.1016/j.jseas.2013.11.010>.
- Stampfli, G.M., and Borel, G.D., 2002, A plate tectonic model for the Paleozoic and Mesozoic constrained by dynamic plate boundaries and restored synthetic oceanic isochrones: Earth and Planetary Science Letters, v. 196, no. 1–2, p. 17–33, [https://doi.org/10.1016/S0012-821X\(01\)00588-X](https://doi.org/10.1016/S0012-821X(01)00588-X).
- Stampfli, G.M., Hochard, C., Verard, C., Wilhem, C., and von Raumer, J., 2013, The formation of Pangea: Tectonophysics, v. 593, p. 1–19, <https://doi.org/10.1016/j.tecto.2013.02.037>.
- Suppe, J., 1983, Geometry and kinematics of fault-bend folding: American Journal of Science, v. 283, no. 7, p. 684–721, <https://doi.org/10.2475/aj.s.283.7.684>.
- Tang, L., 2015, Granites' characteristics and zircon LA-ICP-MS U-Pb dating of Jiling area in Longshoushan, Gansu Province [M.A. thesis] [in Chinese with English abstract]: Nanchang, China, East China Institute of Technology, p. 1–70.
- Tang, W.H., Zhang, Z.C., Li, J.F., Chen, C., and Li, K., 2012, Geochemical characteristics and tectonic significance of the Cretaceous volcanic rocks in the Eastern Terminal of the Altyn Tagh fault zones [in Chinese with English abstract]: Earth Science Frontiers, v. 19, p. 51–62.
- Tang, Y., Zhai, Q.G., Chung, S.L., Hu, P.Y., Wang, J., Xiao, X.C., Song, B., Wang, H.T., and Lee, H.Y., 2020, First mid-ocean ridge-type ophiolite from the Meso-Tethys suture zone in the north-central Tibetan plateau: Geological Society of America Bulletin, v. 132, no. 9–10, p. 2202–2220, <https://doi.org/10.1130/B35500.1>.
- Tappin, P., Meyer, B., Avouac, J.P., Peltzer, G., Gaudemer, Y., Guo, S., Xiang, H., Yin, K., Chen, Z., Cai, S., and Dai, H., 1990, Active thrusting and folding in the Qilian Shan, and decoupling between upper crust and mantle in northeastern Tibet: Earth and Planetary Science Letters, v. 97, p. 382–403, [https://doi.org/10.1016/0012-821X\(90\)90053-Z](https://doi.org/10.1016/0012-821X(90)90053-Z).
- Tappin, P., Xu, Z., Roger, F., Meyer, B., Arnaud, N., Wittlinger, G., and Yang, J., 2001, Oblique stepwise rise and growth of the Tibet Plateau: Science, v. 294, p. 1671–1677, <https://doi.org/10.1126/science.105978>.
- Tseng, C.Y., Yang, H.J., Yang, H.Y., Liu, D., Wu, C., Cheng, C.K., Chen, C.H., and Ker, C.M., 2009, Continuity of the North Qilian and North Qiling orogenic belts,

- Central Orogenic System of China: Evidence from newly discovered Paleozoic adakitic rocks: *Gondwana Research*, v. 16, no. 2, p. 285–293, <https://doi.org/10.1016/j.gr.2009.04.003>.
- van Hinsbergen, D.J., Steinberger, B., Doubrovine, P.V., and Gassmöller, R., 2011, Acceleration and deceleration of India-Asia convergence since the Cretaceous: roles of mantle plumes and continental collision: *Journal of Geophysical Research. Solid Earth*, v. 116, no. B6.
- Vincent, S.J., and Allen, M.B., 1999, Evolution of the Minle and Chaoshui Basins, China: Implications for Mesozoic strike-slip basin formation in Central Asia: *Geological Society of America Bulletin*, v. 111, p. 725–742, [https://doi.org/10.1130/0016-7606\(1999\)111<0725:EOTMA>2.3.CO;2](https://doi.org/10.1130/0016-7606(1999)111<0725:EOTMA>2.3.CO;2).
- Volkmer, J.E., Kapp, P., Guynn, J.H., and Lai, Q., 2007, Cretaceous-Tertiary structural evolution of the north central Lhasa terrane, Tibet: *Tectonics*, v. 26, no. 6, <https://doi.org/10.1029/2005TC001832>.
- Wan, Y.S., Xie, S.W., Yang, C.H., Kröner, A., Ma, M.Z., Dong, C.Y., Du, L.L., Xie, H.Q., and Liu, D.Y., 2014, Early Neoproterozoic (~2.7 Ga) tectono-thermal events in the North China Craton: A synthesis: *Precambrian Research*, v. 247, p. 45–63, <https://doi.org/10.1016/j.precamres.2014.03.019>.
- Wang, A., Liang, T., Li, L., Wang, Z., Fan, C., Wang, Y., Zhang, Y., and Kong, H., 2017, Origin of diagenetic calcite cements in the continental Qaidam Basin, NW China: Implication for fluid flow and hydrocarbon migration: *Journal of Geochemical Exploration*, v. 182, p. 94–109, <https://doi.org/10.1016/j.jexplo.2017.09.002>.
- Wang, C.S., Zhao, X.X., Liu, Z.F., Lippert, P.C., Graham, S.A., Coe, R.S., Yi, H.S., Zhu, L.D., Liu, S., and Li, Y.L., 2008, Constraints on the early uplift history of the Tibetan Plateau: *Proceedings of the National Academy of Sciences of the United States of America*, v. 105, p. 4987–4992, <https://doi.org/10.1073/pnas.0703595105>.
- Wang, W., Zhang, P., Yu, J., Wang, Y., Zheng, D., Zheng, W., Zhang, H., and Pang, J., 2016, Constraints on mountain building in the northeastern Tibet: Detrital zircon records from synorogenic deposits in the Yumen Basin: *Scientific Reports*, v. 6, no. 27604, <https://doi.org/10.1038/srep27604>.
- Wang, X., Chen, L., Ai, Y.S., Xu, T., Jiang, M.M., Ling, Y., and Gao, Y.F., 2018, Crustal structure and deformation beneath eastern and northeastern Tibet revealed by P-wave receiver functions: *Earth and Planetary Science Letters*, v. 497, p. 69–79, <https://doi.org/10.1016/j.epsl.2018.06.007>.
- Wang, Z.Z., Chen, X.H., Li, B., Zhang, Y.P., and Xu, S.L., 2019, The discovery of the Paleoproterozoic syenite in Helishan, Gansu Province, and its implications for the tectonic attribution of the Alxa Block [in Chinese with English abstract]: *Geology in China*, v. 46, p. 1094–1104.
- Wang, Z.Z., Chen, X.H., Shao, Z.G., Li, B., Ding, W.C., Zhang, Y.P., Wang, Y.C., Zhang, Y.Y., Xu, S.L., and Qin, X., 2020, Petrogenesis of the Late Silurian-Early Devonian granites in the Longshoushan-Helishan area, Gansu Province, and its tectonic implications for the Early Paleozoic evolution of the southwestern Alxa Block [in Chinese with English abstract]: *Acta Geologica Sinica*, v. 94, no. 8, p. 2243–2261.
- Wei, Q.Q., Hao, L.B., Lu, J.L., Zhao, Y.Y., Zhao, X.Y., and Shi, H.L., 2013, LA-MC-ICP-MS zircon U-Pb dating of Hexipu granite and its geological implications [in Chinese with English abstract]: *Bulletin of Mineralogy, Petrology and Geochemistry*, v. 32, no. 6, p. 729–735.
- Wu, C.L., Yao, S.Z., Yang, J.S., Zeng, L.S., Chen, S.Y., Li, H.B., Qi, X.X., Wooden, J.L., and Mazzad, F.K., 2006, Double subduction of the Early Paleozoic North Qilian oceanic plate: Evidence from granites in the central segment of North Qilian, NW China [in Chinese with English abstract]: *Geology in China*, v. 33, p. 1197–1208.
- Wu, C.L., Xu, X.Y., Gao, Q.M., Li, X.M., Lei, M., Gao, Y.H., Forst, R.B., and Wooden, J.L., 2010, Early Paleozoic granitoid magmatism and tectonic evolution in North Qilian, NW China [in Chinese with English abstract]: *Yanshi Xuebao*, v. 126, p. 1027–1044.
- Wu, C., Yin, A., Zuza, A.V., Zhang, J.Y., Liu, W.C., and Ding, L., 2016, Pre-Cenozoic geologic history of the central and northern Tibetan Plateau and the role of Wilson cycles in constructing the Tethyan orogenic system: *Lithosphere*, v. 8, p. 254–292, <https://doi.org/10.1130/L494.1>.
- Wu, C., Zuza, A.V., Yin, A., Liu, C.F., Reith, R.C., Zhang, J.Y., Liu, W.C., and Zhou, Z.G., 2017, Geochronology and geochemistry of Neoproterozoic granitoids in the central Qilian Shan of northern Tibet: Reconstructing the amalgamation processes and tectonic history of Asia: *Lithosphere*, v. 9, p. 609–636, <https://doi.org/10.1130/L640.1>.
- Wu, C., Liu, C., Fan, S., Zuza, A.V., Ding, L., Liu, W., Ye, B., Yang, S., and Zhou, Z., 2020a, Structural analysis and tectonic evolution of the western domain of the Eastern Kunlun Range, northwest Tibet: *Geological Society of America Bulletin*, v. 132, p. 1291–1315, <https://doi.org/10.1130/B35388.1>.
- Wu, C., Li, J., Zuza, A.V., Liu, C.F., Liu, W.C., Chen, X.H., Jiang, T., and Li, B., 2020b, Cenozoic cooling history and fluvial terrace development of the western domain of the Eastern Kunlun Range, northern Tibet: *Palaeogeography, Palaeoclimatology, Palaeoecology*, v. 560, no. 109971, <https://doi.org/10.1016/j.palaeo.2020.109971>.
- Wu, F.Y., Zhao, G.C., Wilde, S.A., and Sun, D.Y., 2005, Nd isotopic constraints on crustal formation in the North China Craton: *Journal of Asian Earth Sciences*, v. 24, p. 523–545, <https://doi.org/10.1016/j.jseas.2003.10.011>.
- Wu, F.Y., Ji, W.Q., Wang, J.G., Liu, C.Z., Chung, S.L., and Clift, P.D., 2014, Zircon U-Pb and Hf isotopic constraints on the onset time of India-Asia collision: *American Journal of Science*, v. 314, p. 548–579, <https://doi.org/10.2475/02.2014.04>.
- Xiao, W.J., Windley, B.F., Yong, Y., Yan, Z., Yuan, C., Liu, C.Z., and Li, J.L., 2009, Early Paleozoic to Devonian multiple-accretionary model for the Qilian Shan, NW China: *Journal of Asian Earth Sciences*, v. 35, p. 323–333, <https://doi.org/10.1016/j.jseas.2008.10.001>.
- Xiao, W.J., Windley, B.F., Sun, S., Li, J.L., Huang, B.C., Han, C.M., Yuan, C., Sun, M., and Chen, H.L., 2015, A Tale of amalgamation of three Permo-Triassic collage systems in Central Asia: Orogenies, sutures, and terminal accretion: *Annual Review of Earth and Planetary Sciences*, v. 43, p. 477–507, <https://doi.org/10.1146/annurev-earth-060614-105254>.
- Xiao, W.J., Ao, S.J., Yang, L., Han, C.M., Wan, B., Zhang, J.E., Zhang, Z.Y., Li, R., Chen, Z.Y., and Song, S.H., 2017, Anatomy of composition and nature of plate convergence: Insights for alternative thoughts for terminal India-Eurasia collision: *Science China. Earth Sciences*, v. 60, p. 1015–1039, <https://doi.org/10.1007/s11430-016-9043-3>.
- Xiong, Z.L., Zhang, H.F., and Zhang, J., 2012, Petrogenesis and tectonic implications of the Maozangsi and Huangyanghe granitic intrusions in Lenglongling area, the eastern part of North Qilian Mountains, NW China [in Chinese with English abstract]: *Earth Science Frontiers*, v. 19, no. 3, p. 214–227.
- Xu, Z.Q., Yang, J.S., Zhang, J.X., Jiang, M., Li, H.B., and Cui, J.W., 1999, A comparison between the tectonic units on the two sides of the Altun sinistral strike-slip fault and the mechanism of lithospheric shearing [in Chinese with English abstract]: *Acta Geologica Sinica*, v. 73, p. 193–205.
- Xu, Z.Q., Wang, Q., Li, Z.H., Li, H.Q., Cai, Z.H., Liang, F.H., Dong, H.W., Cao, H., Chen, X.J., Huang, X.M., Wu, C., and Xu, C.P., 2016, Indo-Asian Collision: Tectonic transition from compression to strike slip [in Chinese with English abstract]: *Acta Geologica Sinica*, v. 90, p. 1–23.
- Xue, S., Ling, M.X., Liu, Y.L., Zhang, H., and Sun, W., 2017, The genesis of early Carboniferous adakitic rocks at the southern margin of the Alxa Block, North China: *Lithos*, v. 278–281, p. 181–194, <https://doi.org/10.1016/j.lithos.2017.01.012>.
- Yakovlev, P.V., and Clark, M.K., 2014, Conservation and redistribution of crust during the Indo-Asian collision: *Tectonics*, v. 33, p. 1016–1027, <https://doi.org/10.1002/2013TC003469>.
- Yang, J.S., Xu, Z.Q., Zhang, J.X., Song, S.G., Wu, C.L., Shi, R.D., Li, H.B., and Brunel, M., 2002, Early Paleozoic North Qaidam UHP metamorphic belt on the north-eastern Tibetan plateau and a paired subduction model: *Terra Nova*, v. 14, no. 5, p. 397–404, <https://doi.org/10.1046/j.1365-3121.2002.00438.x>.
- Yang, J.S., Xu, Z.Q., Ma, C.Q., Wu, C.L., Zhang, J.X., Wang, Z.Q., Wang, G.C., Zhang, H.F., Dong, Y.P., and Lai, S.C., 2010, Compound orogeny and scientific problems concerning the Central Orogenic Belt of China [in Chinese with English abstract]: *Geology in China*, v. 37, p. 1–11.
- Yin, A., 2010, Cenozoic tectonic evolution of Asia: A preliminary synthesis: *Tectonophysics*, v. 488, p. 293–325, <https://doi.org/10.1016/j.tecto.2009.06.002>.
- Yin, A., and Harrison, T.M., 2000, *Geologic evolution of the Himalayan-Tibetan Orogen: Annual Review of Earth and Planetary Sciences*, v. 28, p. 211–280, <https://doi.org/10.1146/annurev.earth.28.1.211>.
- Yin, A., and Nie, S.Y., 1996, A Phanerozoic palinspastic reconstruction of China and its neighboring regions, in Yin, A., and Harrison, T.M., eds., *The Tectonic Evolution of Asia*: New York, USA, Cambridge University Press, p. 442–485.
- Yin, A., Rumelhart, P.E., Butler, R., Cowgill, E., Harrison, T.M., Foster, D.A., Ingersoll, R.V., Zhang, Q., Zhou, X.Q., Wang, X.F., Hanson, A., and Raza, A., 2002, Tectonic history of the Altyn Tagh fault system in northern Tibet inferred from Cenozoic sedimentation: *Geological Society of America Bulletin*, v. 114, p. 1257–1295, [https://doi.org/10.1130/0016-7606\(2002\)114<1257:THOTAT>2.0.CO;2](https://doi.org/10.1130/0016-7606(2002)114<1257:THOTAT>2.0.CO;2).
- Yin, A., Manning, C.E., Lovera, O., Menold, C.A., Chen, X., and Gehrels, G.E., 2007, Early Paleozoic tectonic and thermomechanical evolution of ultrahigh-pressure (UHP) metamorphic rocks in the northern Tibetan Plateau, northwest China: *International Geology Review*, v. 49, no. 8, p. 681–716, <https://doi.org/10.2747/0020-6814.49.8.681>.
- Yin, A., Dang, Y.Q., Zhang, L.C., Jiang, W.M., Zhou, S.P., Chen, X.H., Gehrels, G.E., and McRivette, M.W., 2008a, Cenozoic tectonic evolution of Qaidam basin and its surrounding regions (Part 1): The southern Qilian Shan-Nan Shan thrust belt and northern Qaidam basin: *Geological Society of America Bulletin*, v. 120, p. 813–846, <https://doi.org/10.1130/B26180.1>.
- Yin, A., Dang, Y.Q., Zhang, M., Chen, X.H., and McRivette, M.W., 2008b, Cenozoic tectonic evolution of the Qaidam basin and its surrounding regions (Part 3): Structural geology, sedimentation, and regional tectonic reconstruction: *Geological Society of America Bulletin*, v. 120, p. 847–876, <https://doi.org/10.1130/B26232.1>.
- Yu, J.X., Pang, J.Z., Wang, Y.Z., Zheng, D.W., Liu, C.C., Wang, W.T., Li, Y.J., Li, C.P., and Xiao, L., 2019, Mid-Miocene uplift of the northern Qilian Shan as a result of the northward growth of the northern Tibetan Plateau: *Geosphere*, v. 15, p. 423–432, <https://doi.org/10.1130/GES01520.1>.
- Yu, X.L., Cai, C.L., Zhang, S.L., Wei, X.L., and Liu, X.X., 2018, Petrogenesis of Early Silurian intrusive rocks in Yenuijishan Area of South Qilian: Constraints from geochemistry and LA-ICP-MS zircon U-Pb geochronology [in Chinese with English abstract]: *Northwest Geology*, v. 51, no. 4, p. 134–146.
- Zhai, M.G., and Santosh, M., 2011, The early Precambrian odyssey of the North China Craton: A synoptic overview: *Gondwana Research*, v. 20, p. 6–25, <https://doi.org/10.1016/j.gr.2011.02.005>.
- Zhang, H.P., Zhang, P.Z., Prush, V., Zheng, D.W., Zheng, W.J., Wang, W.T., Liu, C.C., and Ren, Z.K., 2017a, Tectonic geomorphology of the Qilian Shan in the northeastern Tibetan Plateau: Insights into the plateau formation processes: *Tectonophysics*, v. 706–707, p. 103–115, <https://doi.org/10.1016/j.tecto.2017.04.016>.
- Zhang, J.J., Wang, T., Zhang, L., Tong, Y., Zhang, Z.C., Shi, X.J., Guo, L., Huang, H., Wang, Q.D., Huang, W., Zhao, J.X., Ye, K., and Hou, J.Y., 2015, Tracking deep crust by zircon xenocrysts within igneous rocks from the northern Alxa, China: Constraints on the southern boundary of the Central Asian Orogenic Belt: *Journal*



- of Asian Earth Sciences, v. 108, p. 150–169, <https://doi.org/10.1016/j.jseas.2015.04.019>.
- Zhang, L.Q., Zhang, H.F., Zhang, S.S., Xiong, Z.L., Luo, B.J., Yang, H., Pan, F.B., Zhou, X.C., Xu, W.C., and Guo, L., 2017b, Lithospheric delamination in post-collisional setting: Evidence from intrusive magmatism from the North Qilian orogen to southern margin of the Alxa block, NW China: *Lithos*, v. 288–289, p. 20–34, <https://doi.org/10.1016/j.lithos.2017.07.009>.
- Zhang, J.X., and Gong, J.H., 2018, Revisiting the nature and affinity of the Alxa Block [in Chinese with English abstract]: *Yanshi Xuebao*, v. 34, p. 940–962.
- Zhang, X. Y., Wang, C. T., OUYANG, W. G., and Li, R.B., 2018, Zircon U-Pb ages and their geological significance of Aogutun-wulan pluton in South Qilian, China [in Chinese with English abstract]: *Journal of Earth Sciences and Environment*, v. 40, no. 5, p. 546–562.
- Zhang, Z.Q., Wang, K.X., Wang, G., Liu, X.D., Liu, W.H., and Wu, B., 2021, Petrogenesis and tectonic significances of the Paleozoic Jiling syenite in the Mountain Longshou area, Gansu province [in Chinese with English abstract]: *Dizhi Lunping*, v. 64, no. 4, p. 1017–1029.
- Zhao, G.C., Sun, M., Wilde, S.A., and Li, S.Z., 2005, Late Archean to Paleoproterozoic evolution of the North China Craton: Key issues revisited: *Precambrian Research*, v. 136, p. 177–202, <https://doi.org/10.1016/j.precamres.2004.10.002>.
- Zhao, G.C., Wilde, S.A., Guo, J.H., Cawood, P.A., Sun, M., and Li, X.P., 2010, Single zircon grains record two Paleoproterozoic collisional events in the North China Craton: *Precambrian Research*, v. 177, p. 266–276, <https://doi.org/10.1016/j.precamres.2009.12.007>.
- Zhao, G.C., Cawood, P.A., Li, S.Z., Wilde, S.A., Sun, M., Zhang, J., He, Y.H., and Yin, C.Q., 2012, Amalgamation of the North China Craton: Key issues and discussion: *Precambrian Research*, v. 222–223, p. 55–76, <https://doi.org/10.1016/j.precamres.2012.09.016>.
- Zhao, J.M., Mooney, W.D., Zhang, X.K., Li, Z.C., Jin, Z.J., and Okaya, N., 2006, Crustal structure across the Altyn Tagh Range at the northern margin of the Tibetan plateau and tectonic implications: *Earth and Planetary Science Letters*, v. 241, p. 804–814, <https://doi.org/10.1016/j.epsl.2005.11.003>.
- Zhao, Z.B., Bons, P.D., Stübner, K., Wang, G.H., and Ehlers, T.A., 2017, Early Cretaceous exhumation of the Qiangtang Terrane during collision with the Lhasa Terrane, Central Tibet: *Terra Nova*, v. 29, p. 382–391, <https://doi.org/10.1111/ter.12298>.
- Zhao, Z.B., Bons, P.D., Li, C., Wang, G.H., Ma, X.X., and Li, G.W., 2020, The Cretaceous crustal shortening and thickening of the South Qiangtang Terrane and implications for proto-Tibetan Plateau formation: *Gondwana Research*, v. 78, p. 141–155, <https://doi.org/10.1016/j.gr.2019.09.003>.
- Zhang, R.G., Wu, T.R., Zhang, W., Xu, C., Meng, Q.P., and Zhang, Z.Y., 2014, Late Paleozoic subduction system in the northern margin of the Alxa block, Altaids: Geochronological and geochemical evidences from ophiolites: *Gondwana Research*, v. 25, p. 842–858, <https://doi.org/10.1016/j.gr.2013.05.011>.
- Zheng, Y.D., and Zhang, Q., 1994, The Yagan metamorphic core complex and extensional detachment fault in Inner Mongolia, China: *Acta Geologica Sinica*, v. 68, p. 1145–1154.
- Zhou, X.C., Zhang, H.F., Luo, B.J., Pan, F.B., Zhang, S.S., and Guo, L., 2016, Origin of high Sr/Y-type granitic magmatism in the southwestern of the Alxa Block, Northwest China: *Lithos*, v. 256–257, p. 211–227, <https://doi.org/10.1016/j.lithos.2016.04.021>.
- Zuza, A.V., and Yin, A., 2016, Continental deformation accommodated by non-rigid passive bookshelf faulting: An example from the Cenozoic tectonic development of northern Tibet: *Tectonophysics*, v. 677–678, p. 227–240, <https://doi.org/10.1016/j.tecto.2016.04.007>.
- Zuza, A.V., Cheng, X., and Yin, A., 2016, Testing models of Tibetan Plateau formation with Cenozoic shortening estimates across the Qilian Shan-Nan Shan thrust belt: *Geosphere*, v. 12, p. 501–532, <https://doi.org/10.1130/GES01254.1>.
- Zuza, A.V., Wu, C., Reith, R.C., Yin, A., Li, J., Zhang, J., Zhang, Y., Wu, L., and Liu, W., 2018, Tectonic evolution of the Qilian Shan: An early Paleozoic orogen reactivated in the Cenozoic: *Geological Society of America Bulletin*, v. 130, p. 881–925, <https://doi.org/10.1130/B31721.1>.
- Zuza, A.V., Wu, C., Wang, Z., Levy, D.A., Li, B., Xiong, X., and Chen, X., 2019, Underthrusting and duplexing beneath the northern Tibetan Plateau and the evolution of the Himalayan-Tibetan orogen: *Lithosphere*, v. 11, p. 209–231, <https://doi.org/10.1130/L1042.1>.

SCIENCE EDITOR: ROB STRACHAN  
ASSOCIATE EDITOR: ZHENG-XIANG LI

MANUSCRIPT RECEIVED 16 OCTOBER 2020  
REVISED MANUSCRIPT RECEIVED 16 MARCH 2021  
MANUSCRIPT ACCEPTED 5 APRIL 2021

Printed in the USA